SANDIA REPORT

SAND2013-8112
Unlimited Release
Printed September 2013

Using Fast Neutron Signatures for Improved UF_6 Cylinder Enrichment Measurements

Scott D. Kiff
Erik Brubaker
Mark Gerling
Peter Marleau
Wondwosen Mengesha

Prepared by:
Sandia National Laboratories
Albuquerque, New Mexico 87185 and Livermore, California 94550

Sandia National Laboratories is a multi-program laboratory managed and operated by Sandia Corporation, a wholly owned subsidiary of Lockheed Martin Corporation, for the U.S. Department of Energy's National Nuclear Security Administration under contract DE-AC04-94AL85000.

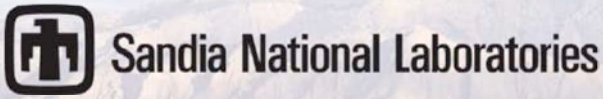

Issued by Sandia National Laboratories, operated for the United States Department of Energy by Sandia Corporation.

Available to DOE and DOE contractors from
U.S. Department of Energy
Office of Scientific and Technical Information
P.O. Box 62
Oak Ridge, TN 37831

Telephone: (865) 576-8401
Facsimile: (865) 576-5728
E-Mail: reports@adonis.osti.gov
Online ordering: http://www.osti.gov/bridge

Available to the public from
U.S. Department of Commerce
National Technical Information Service
5285 Port Royal Rd.
Springfield, VA 22161

Telephone: (800) 553-6847
Facsimile: (703) 605-6900
E-Mail: orders@ntis.fedworld.gov
Online order: http://www.ntis.gov/help/ordermethods.asp?loc=7-4-0#online

SAND2013-8112
Unlimited Release
Printed September 2013

Using Fast Neutron Signatures for Improved UF_6 Cylinder Enrichment Measurements

Scott D. Kiff, Erik Brubaker, Mark Gerling, Peter Marleau
Radiation and Nuclear Detection Systems

Wondwosen Mengesha
Cyber-Physical Systems

Sandia National Laboratories
P.O. Box 969, MS9406
Livermore, California 94551-0969

Abstract

The authors have investigated the use of fast neutrons—primarily the fast neutron energy spectrum—as a signature for uranium hexafluoride (UF_6) nuclear accountancy measurements. Detailed modeling of UF_6 storage cylinders and a proposed neutron detection system indicates that the measured neutron energy spectrum is indeed a function of uranium enrichment. Field measurements at the Department of Energy's Paducah Gaseous Diffusion Plant with a detection system similar to the modeled system provided an opportunity to collect signatures from several storage cylinders containing UF_6 with a range of enrichments. Subsequent analysis lends credibility to the modeling results, indicating that enrichment over the range measured (0.72% to 4.95% uranium-235) can be extracted from the measured neutron energy spectrum. These results were scaled to estimate the tradeoff in measurement system size and counting time to achieve a relative enrichment measurement uncertainty of 5%.

ACKNOWLEDGMENTS

The authors would like to thank several individuals for their contributions to this project. Robert Cooper provided modeling support for the simulated emissions of 30B cylinders, and played an important role in experiments and analysis of the detector response. Laura Kogler provided important analysis support, and generated important comparisons of the Neutron Scatter Camera to other mature technologies. Isaac Shokair was very helpful in understanding implementation of the Principal Component Analysis technique. Michael Streicher provided important simulation and experimental support, which was useful in understanding the detector response to 30B emissions and the characterization of hardware in the laboratory.

Jim Brennan and Dan Throckmorton provided support during the assembly of the detector system fielded at the Paducah Gaseous Diffusion Plant (PGDP). Stanley Mrowka provided software for the data acquisition system and assisted in the data collection at PGDP. Randy DeVault (DOE/Oak Ridge Field Office) and Richard Mayer (DOE/Lexington Field Office) were instrumental in identifying and facilitating the measurement opportunity at PGDP. Brent Montgomery, John Price, and Tullus Crawford of the United States Enrichment Corporation (USEC) provided support for the PGDP measurements.

Prof. Sara Pozzi, Shaun Clarke, Marek Flaska, Christopher Lawrence, Marc Paff, and Eric Miller (all of the University of Michigan's Detection for Nuclear Nonproliferation Group) were informal collaborators on this effort, and provided interesting technical expertise and feedback during the course of the project.

This work was funded by the Sandia Laboratory Directed Research and Development office under the title "Using Fast Neutron Signatures for Improved UF_6 Cylinder Enrichment Measurements". The authors would also like to thank the NNSA NA-24 Human Capital Development fund for support related to the PGDP data collection and analysis effort.

CONTENTS

TABLES

FIGURES

NOMENCLATURE

AUC	area under curve
cm	centimeter
FPP	false positive probability
keV	kilo-electron volt
kg	kilogram
LANL	Los Alamos National Laboratory
lb	pound
m	meter
MeV	mega-electron volt
MeVee	MeV electron equivalent
NDA	non-destructive assay
NSC	Neutron Scatter Camera
PCA	principal component analysis
PD	probability of detection
PGDP	Paducah Gaseous Diffusion Plant
PHS	pulse-height spectrum
PMT	photomultiplier tube
PSD	pulse-shape discrimination
ROC	receiver-operating characteristic
SF	spontaneous fission
SNL	Sandia National Laboratories
UF_6	uranium hexafluoride
USEC	United States Enrichment Corporation

1. INTRODUCTION

Safeguards activities at uranium enrichment facilities require accurate, independent measurements of uranium mass for each uranium hexafluoride (UF_6) cylinder with contents that are either a process input or output. Current technology tends to rely upon gamma measurements or both passive and active thermal neutron counting using ^{3}He detectors [1].

The most common and classic gamma-ray technique used for assaying UF_6 cylinders is based upon the detection of the characteristic 186 keV gamma-ray from ^{235}U and is known as the enrichment meter [2]. Although this technique is a direct enrichment measurement approach, it is highly constrained by a priori assumption of uniform UF_6 mass distribution within the storage cylinder; since the measurement is only sensitive to the UF_6 mass within a few millimeters of the wall of the storage cylinder (see Figure 1.1), geometrical perturbations can impact a measurement. Corrections must also be applied to account for the absorption of the 186 keV gamma rays within the container wall and any mass between the detector and the UF_6 such as surface deposits, referred to as heel, from previous use of the storage container. Measurement uncertainty associated with the absorber mass between the detection medium and the UF_6 can reach 6% [1]. High energy gamma-ray techniques may provide the advantage of assaying the entire UF_6 volume due to reduced self-absorption. However, it has been observed that biasing from impurities found in the heel may impact the quality of data using these techniques [3-4].

Passive neutron assay techniques can be based on simple counting of the thermalized neutron flux originating from the UF_6 cylinders [5], or may also consider the time dispersion of neutron counts for a multiplicity analysis [6]. Very few neutrons are generated directly from ^{235}U in UF_6; instead, most neutrons are generated from ^{238}U spontaneous fission or ^{234}U and ^{238}U alpha-decay processes. Thermal neutron methods are also sensitive to geometrical perturbations of the UF_6 within the cylinder, giving rise to potentially significant systematic measurement uncertainties [3]. Given the short path length of low-energy gammas and neutrons through UF_6, these methods may also be insensitive to material in the center of the cylinder (see Figure 1.1). In the context of international safeguards, for which coordinated state-level diversion is a theoretical possibility, it is undesirable to rely upon either gamma-ray or thermal neutron measurement techniques that are effectively measurements of the outer material skin, blind to the central contents.

Active neutron assay techniques are based on thermal neutron probing of the UF_6 mass and the detection of induced fission neutrons from ^{235}U [7]. Unlike the passive approach, the active neutron approach is a direct measurement of ^{235}U content. However, application of the active technique in unattended measurements is difficult and requires special detection geometry [1]. Current active approaches are designed with the neutron detector in contact with the UF_6 cylinder to allow better detection efficiency. These approaches, however, may not be supported in unattended measurements where a minimum stand-off distance is required for safe movement of the UF_6 cylinders.

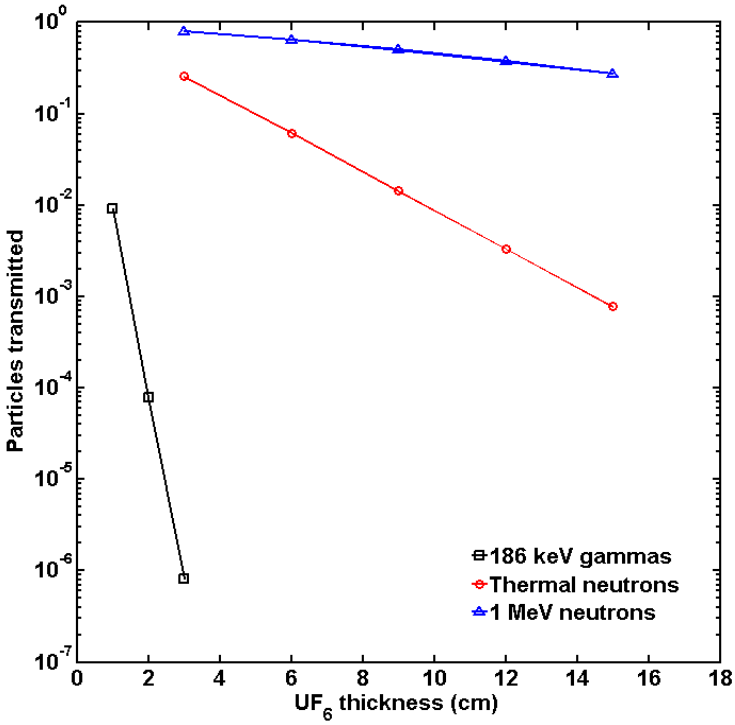

Figure 1.1. A Monte Carlo calculation of the particles transmitted through a given thickness of UF6 up to a maximum thickness expected for a uniform material loading in a 30B cylinder. All calculations consider a beam of incident particles normal to a slab of UF6. Neutron measurements do not consider the effects of induced fission. High-energy neutrons have far superior sensitivity to material in the center of a cylinder.

This document reports on a Sandia investigation of the use of fast neutron spectrometers to augment the measurement capabilities surrounding UF_6 cylinder verification. Neutron spectrometry allows for direct calculation of total mass and enrichment because the processes that generate neutrons in the UF_6 have unique energy distributions and are functions of the uranium isotopics [1]. Two of these processes are spontaneous fission in ^{238}U (neutrons extending to about 10 MeV) and neutrons produced by bombardment of ^{234}U and ^{238}U decay αs upon fluorine, which terminate at about 2.5 MeV. These neutrons are generated by the inherent radioactive decay of the material, and occur independently of material geometry. Figure 1.2 shows the contributions of spontaneous fission and (α,n) neutrons to the UF_6 neutron spectrum. The third process is induced fission in ^{235}U, which has a slightly different energy distribution than spontaneous fission and is a function of not only material enrichment and mass, but also geometry. The technique relies upon an underlying assumption of constant ^{235}U/ ^{234}U ratio so that the measured neutron flux is linear with ^{235}U enrichment.

Although the processes that generate neutrons in UF_6 samples are readily acknowledged [8], neutron spectrometry has not been directly applied as a tool to independently measure ^{238}U and ^{235}U content of 30B cylinders. This technique has two strong advantages: first, it relies upon the measurement of highly-penetrating particles, making it possible to sample the entire UF_6 volume; second, using neutron spectrometry to determine the spontaneous fission and (α,n) components can provide an independent measurement enrichment and total mass.

This report reviews the body of work performed to study the application of neutron spectrometry to UF_6 cylinder enrichment measurements. First is a presentation of the neutron production and transport simulations to understand how transport processes (scattering, induced fission, and self-absorption) in the UF_6 modify the energy spectrum. This is followed by a study of detector response and analysis of the simulations. Experimental confirmation of these computational results via measurements of UF_6 cylinders at an enrichment facility were performed, and are discussed. Finally, a review of some passive imaging work and a summary of the project are presented.

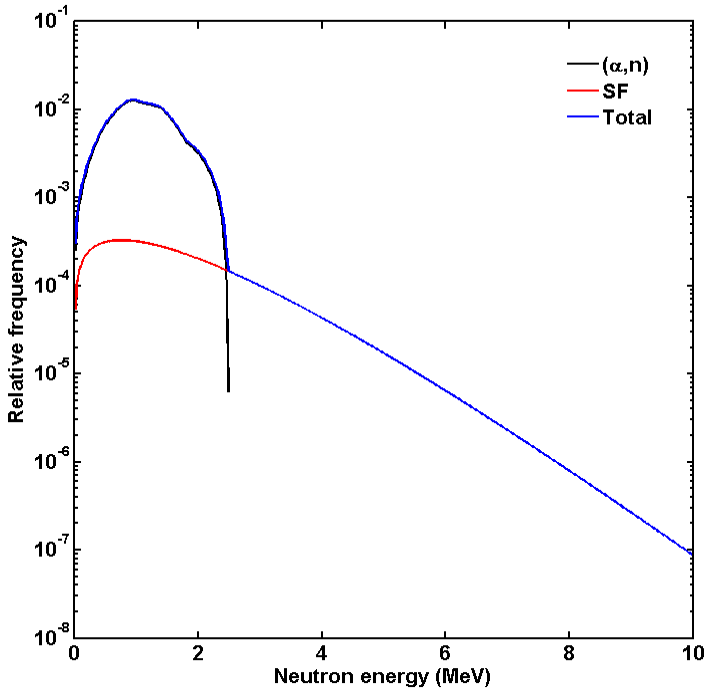

Figure 1.2. A plot of the neutron spectral components for 5% enriched UF_6. The ^{234}U (α,n) reaction on fluorine generates a peaked neutron spectrum that terminates abruptly near 2.5 MeV. The ^{238}U spontaneous fission spectrum peaks near this upper boundary, and extends out to about 10 MeV. Placing an energy cut at 2.5 MeV will allow separation of the two contributions to the neutron source term.

2. SIMULATION OF THE NEUTRON ENERGY SPECTRUM

2.1 Uranium hexafluoride emissions

The principal goal of this project is to take advantage of changes in the neutron energy spectrum arising from the degree of uranium enrichment. Therefore, before even considering the detector response function, it is useful to study the pure neutron spectrum emitted from the cylinder, and how the original spectrum is altered by scattering, attenuation, and induced fission in the cylinder. It is possible that the differences in the spectrum can be washed out by these processes, making the neutron spectrometry technique unusable in practice—although from initial calculations it does appear that the spectral differences remain sufficient for neutron spectrometry to continue to be pursued as a viable enrichment measurement technique.

The neutron emission spectra calculated for this study use the isotopics presented in Berndt [1] for depleted uranium hexafluoride (DU), natural uranium (^{nat}U), and uranium enriched to 5% ^{235}U (LEU). Any additional simulated ^{235}U enrichments use a ^{234}U isotopic fraction that is linearly interpolated from the Berndt data table. The success of this measurement technique is highly dependent upon a predictable ^{234}U/^{235}U isotopic ratio, as the technique is an indirect measurement of ^{235}U enrichment due to the significant fraction of neutrons that come from isotopes other than ^{235}U. Fortunately, in mass-based enrichment processes (such as gaseous diffusion and centrifuge enrichment), the ^{234}U is enriched at the same time as the ^{235}U; Los Alamos National Laboratory (LANL) experiments indicate that the ratio of these two isotopes remains fixed through low enrichments (up to 5% ^{235}U) [9], which is the primary enrichment range of interest for commercial reactor fuel.

The modeled material density is 4.6 g/cm^3 [10], which was obtained from an Argonne National Laboratory webpage but is less than the often-assumed 5.1 g/cm^3. Since the mass of material is fixed for all calculations (and not the volume), the impact on the source neutron rate and spectrum is expected to be negligible.

SOURCES 4C [11] is a LANL-developed code for calculating neutron energy spectra and source intensities. It uses data libraries and α-particle transport calculations to determine the spontaneous fission and (α,n) source term contributions. It is used to calculate the spontaneous fission and (α,n) spectral contributions. The SOURCES 4C calculated spectral contributions are presented in Figure 2.1.

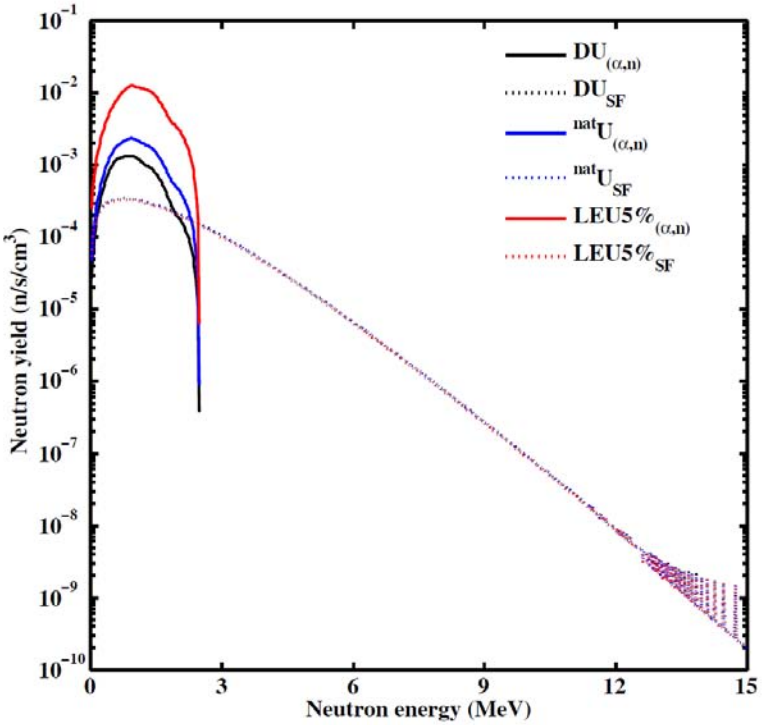

Figure 2.1. The (α,n) and spontaneous fission (SF) contributions to the neutron energy spectrum for three enrichment levels of UF_6, plotted separately. The spontaneous fission spectral contributions are nearly identical for each enrichment, since the total ^{238}U mass is approximately constant. However, the (α,n) contribution varies by over an order of magnitude, changing the total energy spectrum in a quantifiable manner.

2.2 Type 30B storage cylinder emissions

Type 30B storage cylinders are common at enrichment facilities. They can be loaded with up to 5020 lb (2282 kg) of UF_6 enriched at or below 5% ^{235}U [12], so they are useful for storing enriched product to be used at commercial reactors. A second common storage cylinder is the 48Y cylinder, which is primarily used for storing depleted uranium product. 48Y cylinders can be loaded with 27,560 lb (12,527 kg) of UF_6.

To calculate the degradation of the energy spectra via scattering, capture, and induced fission in the UF_6, the SOURCES 4C spectra are inserted into an MCNP5 [13] model of a 30B cylinder [12]. This model considers a maximum loading of UF_6 at a density of 4.6 g/cm^3 with a uniform distribution of material in a thick shell. The gas space in the cylinder is modeled at a vacuum, and no environmental features (such as soil) are included in this basic model. Since the modeled measurement instrument (the Neutron Scatter Camera) has 12.7-cm right cylinders as detection volumes at a standoff of 1 m, a tally of the neutron spectrum crossing a 12.7 cm disk at a standoff of 1 m was calculated. The detector system and the detector response calculations will be discussed in a later section of this report.

Source neutrons are distributed uniformly through the portion of the cylinder that is occupied by solid UF_6, with isotropic direction sampling and energy sampled from the SOURCES 4C spectrum corresponding to the modeled ^{235}U enrichment. A simplification is made with the

assumption that all neutrons can be sampled independently of one another. This is correct for (α,n) neutrons, as there is only one neutron per α-decay and those are distributed uniformly throughout the UF_6. However, this is not exactly correct for spontaneous fission neutrons; fission generates neutrons in multiples, and a correct treatment would sample a random starting point for a fission, then independently sample the number of fission neutrons to create at this fission location and each neutron's energy from appropriate distributions. Since the detection scheme measures single particle energies (i.e., does not rely upon detecting coincident particles) and the solid angle coverage is small at the 1 m standoff (neutrons would not likely interact in coincidence in the detector, creating pileup), the simplified treatment is not expected to introduce a significant perturbation in the simulated neutron energy spectrum.

The first simulation considered vacuum in the volumes occupied by UF_6 and steel; this case calculates the unperturbed neutron contributions at the tally location, since there are no materials for neutron interactions. In sequence, the next simulation considered turning the 30B cylinder volume back to steel, then the source volume into UF_6 (but without induced fission). These two simulations demonstrate the effect of neutron scattering in real materials. Finally, prompt fission and then delayed fission contributions were added. Figure 2.2 displays the results of this study. The biggest effect seems to be scattering of high-energy neutrons by UF_6, followed by down-scattering on steel and induced fission. Note that this particular simulation set considered natural uranium (0.72% ^{235}U); at this ^{235}U content, induced fission contributions are expected to be quite small.

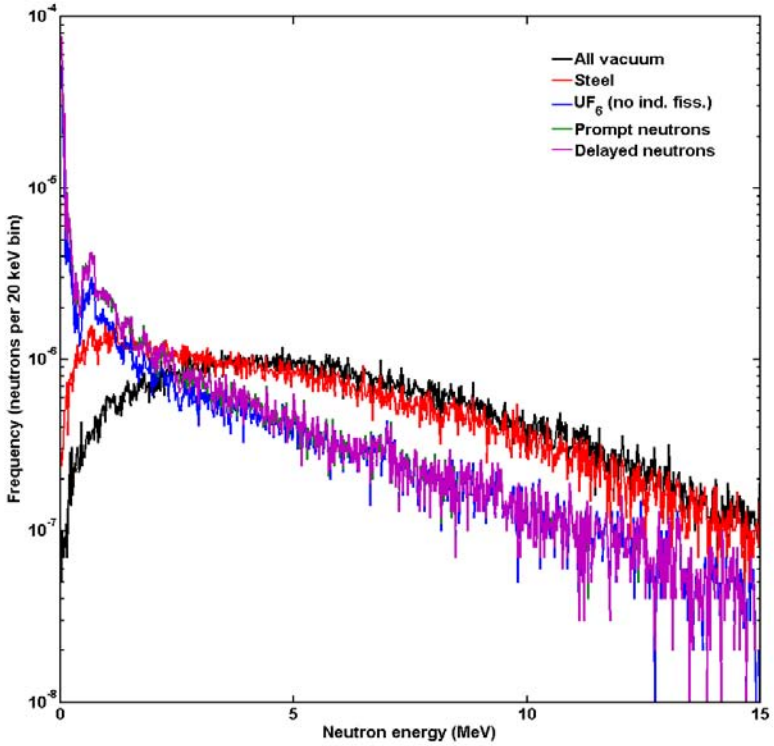

Figure 2.2. The effects of scattering, capture, and induced fission on the neutron energy spectrum emitted from the cylinder for a $^{nat}UF_6$ source.

Simulations of each of the three enrichments considered were run in the MCNP5 model using a number of starting neutrons corresponding to a very long measurement (10 h) for good statistics. (Note that the number of starting neutrons was different for each simulation, as the (α,n) intensity increases with enrichment due to the larger concentration of ^{234}U.) The tallied neutron flux through a 12.7 cm-diameter detector face at a standoff of 1 m is plotted in Figure 2.3. The differences in the neutron spectra, especially in the region under about 2.5 MeV, are evident in this plot. This indicates that the neutron spectrum emitted from the surface of the 30B cylinder is a function of uranium enrichment, although it does not yet account for the detector response function.

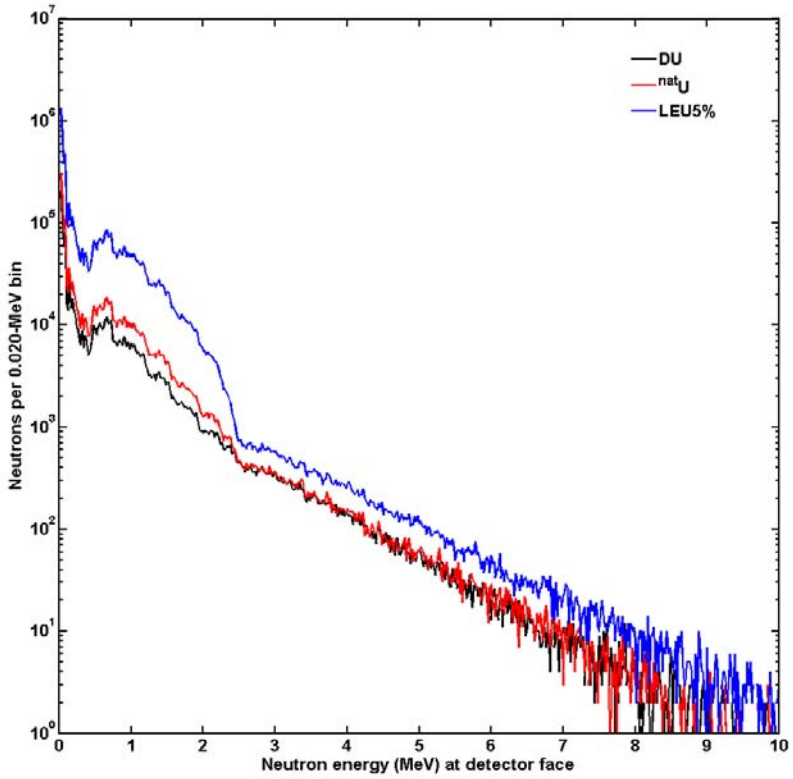

Figure 2.3. The calculated neutron flux entering a single 12.7 cm-diameter detector element at a standoff of 1 m.

2.3 Detector response modeling

The detector response modeling considers the use of the Neutron Scatter Camera (NSC) [14], developed at Sandia. The Neutron Scatter Camera utilizes two planes of Eljen EJ-309 organic liquid scintillator cells to detect neutrons, discriminate them from photons, and tag each interaction with its location (center of detecting cell), interaction time, and measured pulse height. All of this information can then be used to generate pulse height distributions for individual cells in the array and for double-scatter events between two distinct cells.

The NSC is an attractive neutron spectrometer for this application. Its large volume of dense liquid scintillator means high neutron detection efficiency. The ability to discriminate neutrons from photons using pulse shape discrimination (PSD) is important because of the large photon

flux emitted from a 30B cylinder. The NSC has two inherent modes of neutron spectroscopy, single-scatter (more efficient) and double-scatter (less degradation from the incident neutron energy distribution), and can perform neutron imaging using the double-scatter subset of interactions. Finally, the NSC is advantageous because Sandia has two functioning NSCs with sophisticated modeling capability supporting each system. The modeling is described in some detail in a peer-reviewed publication [15], and will not be repeated here.

Two simulations were run, natural enrichment and 5% ^{235}U enrichment; the 32-cell NSC was centered along the cylinder side for each enrichment case, with a standoff of 1 m from the cylinder surface. The measured double-scatter spectrum was tallied, and is shown for each enrichment in Figure 2.4. This plot demonstrates a difference in the observed neutron energy measurement, as the large increase in (α,n) neutron production with increasing enrichment leads to an increase in the observed measurement around 2 MeV. It should be noted that the double-scatter mode is highly inefficient, as it requires a neutron to interact in two different cells and deposit enough energy in each cell (above ~0.5 MeV) for the PSD classifier to be able to determine each interaction to be from a neutron. As a rule of thumb for the NSC, the single-scatter mode produces neutron events increased by a factor of *O*(100).

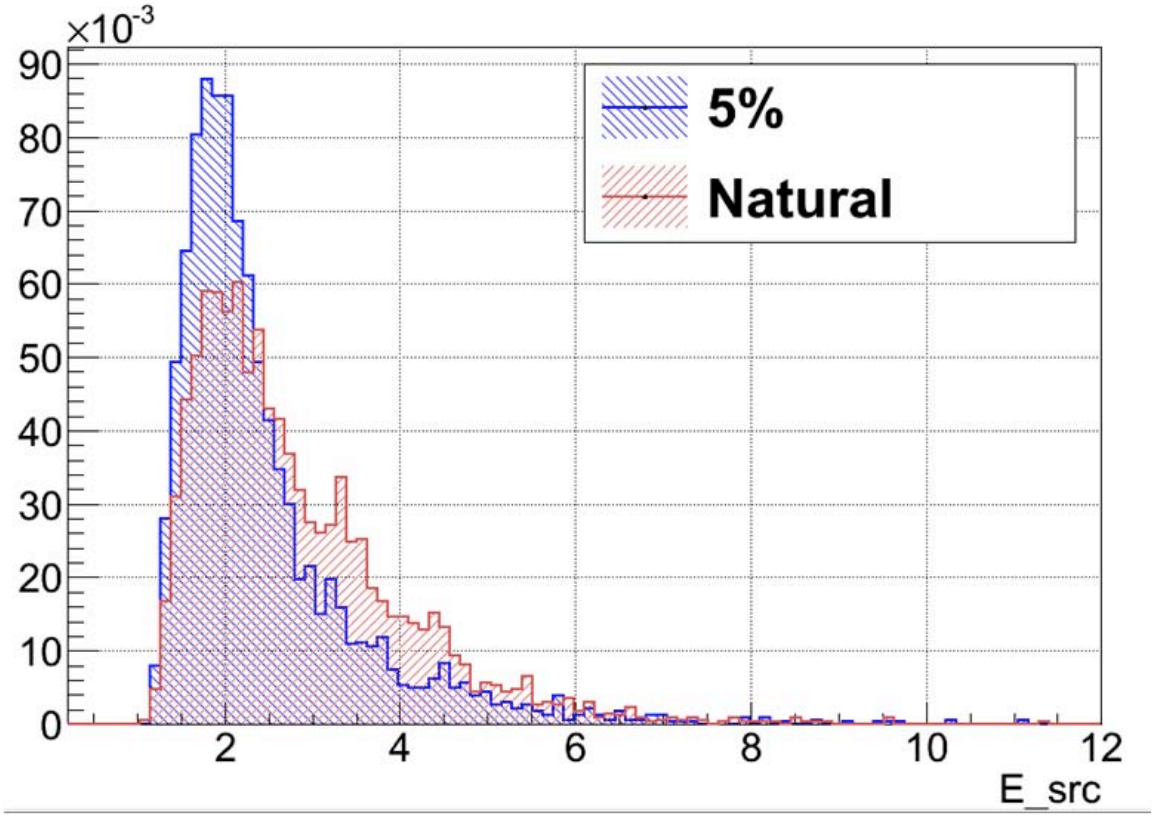

Figure 2.4. The reconstructed double-scatter spectrum from the 32-cell Neutron Scatter Camera for two enrichments, natural and 5% ^{235}U. The abscissa (labeled E_src) is the reconstructed neutron energy, in units of MeV. The ordinate is the frequency of each neutron energy bin.

2.4 Comparisons against other neutron detectors

With simulated detector response in hand, it is now possible to perform a quick comparison of NSC performance against a mature 30B nondestructive assay (NDA) system. The system chosen is UCAS, the Uranium Cylinder Assay System designed by LANL [5]. UCAS is a ^{3}He-based neutron counting system, and therefore presents an interesting technology alternative for passive neutron counting of 30B cylinders.

Figure 2.5 presents the reported UCAS count rate as a function of ^{235}U enrichment, and the sum over all 32 NSC cells for single-cell events, applying a 700 keV threshold for neutron classification. A simple assumption is that the detectors should produce similar count rates to achieve similar measurement uncertainty in a fixed measurement time, although due to the differences in analysis techniques this may not be strictly true. It appears that the UCAS system has a much higher count rate. There are three factors that can be considered for detection rate improvement. The first is simply a modeling assumption—the LANL reported source neutron rate is universally higher than the rate used for the NSC simulations, and for 5% enrichment is almost 50% higher. The second is the neutron counting threshold for the NSC. Figure 2.6 presents the cumulative distribution of neutron counts as a function of threshold. Reducing the threshold from 700 keV to 200 keV would increase the NSC counts by nearly an order of magnitude. Finally, the UCAS standoff distance is not noted in the reference paper, but it is likely much shorter than 1 m. Placing the NSC closer to the 30B cylinder would increase the interaction rates.

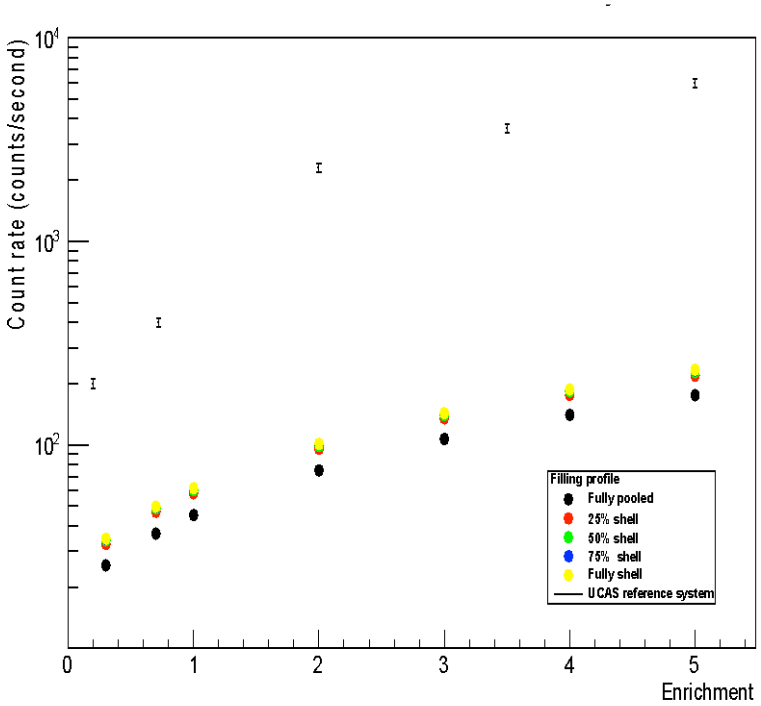

Figure 2.5. Count rate as a function of enrichment for UCAS (small black markers with error bars) and the NSC (thick colored symbols denoting different geometries of the solidified UF_6). The NSC energy threshold is set at 700 keV.

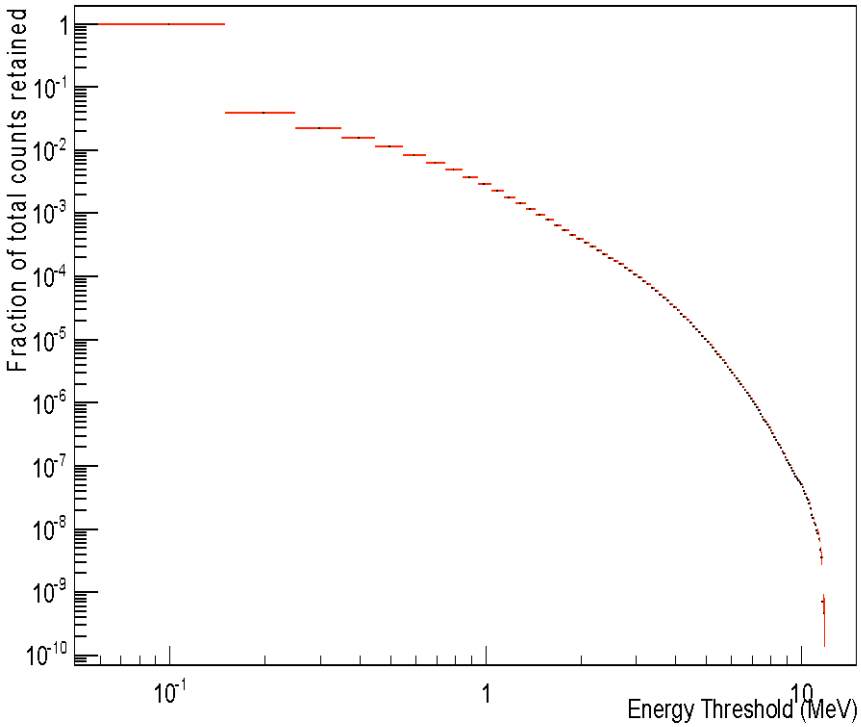

Figure 2.6. The cumulative distribution of NSC single-cell counts as a function of energy threshold.

2.5 Discussion

The simulations reported in this section build from simple modeling of the UF_6 source neutrons to 30B simulations with full transport phenomena to detector response modeling. These simulations indicate that the UF_6 neutron energy spectrum is indeed a function of uranium enrichment, and simulations including full NSC response produce visibly different spectral distributions.

Figure 2.5 indicates that the geometry of the UF_6 can have an impact on the measured count rates. Although the figure does not indicate whether the neutron energy distributions are a function of geometry, this is still an undesirable result. The analysis technique explored in the next section is intended to filter out geometry effects.

The NSC count rate is lower than that of a fielded thermal neutron counting system, the UCAS. Increasing the count rate may be accomplished by using a lower energy threshold if possible, although there is a limit dictated by the desired PSD performance of the detector. The count rate may also be increased by moving the detector closer to the 30B cylinder, or by increasing the size of the detection array (a larger NSC).

The NSC is not the only neutron spectrometer that could be considered for this application, but its combination of detection efficiency, gamma-ray rejection, and spectroscopy performance make it an attractive option.

3. ANALYSIS OF THE NEUTRON ENERGY SPECTRUM

3.1 Motivation

The UF_6 neutron spectrum is comprised of three major components from distinct processes that generate the neutron population in UF_6: spontaneous fission (SF) neutrons from ^{238}U; neutrons produced by $^{19}F(\alpha,n)^{22}Na$ nuclear reactions of alpha particles, from the decay of ^{234}U and ^{238}U, with fluorine atoms; and induced fission neutrons resulting from fission reactions. The relative contribution of these processes causes features in the observed neutron spectrum that are functions of the ^{235}U enrichment in the UF_6. However, these spectral features may not be visibly identifiable since they are smeared in the measured neutron pulse-height spectrum. This is mainly true when using organic scintillators, such as liquid scintillators, for neutron spectrometry. Although liquid scintillators are the favored for their superior neutron-gamma pulse shape discrimination (PSD), it would be difficult to readily discriminate the enrichment-related features in the observed neutron spectrum due to their poor energy resolution. A sensitive method is necessary to identify intrinsic features attributed to the detected neutron spectrum and therefore enable discrimination and verification of the UF_6 enrichment. The conceptual framework in the present study is that for a given declared UF_6 enrichment, the measured neutron spectrum has characteristic features related to the enrichment. Departure from these expected features indicates anomaly and with a proper metric defined, the corresponding enrichment can possibly be identified.

This section presents an investigation made using simulated neutron spectra and Principal Component Analysis (PCA) to discriminate spectral attributes that can be used for unattended and passive characterization of UF_6 enrichment in 30B storage cylinders. The MCNP5 [13] and Geant4.9.4 [16] Monte Carlo transport codes were used to model the neutron transport through the 30B cylinder and then through liquid scintillator cells used for the neutron spectrum detection. Liquid scintillator cells were chosen as the passive neutron spectrometry detectors due to their high neutron detection efficiency and effective neutron-gamma PSD that is crucial in neutron spectrum feature identification using the PCA technique. The PCA technique has proven to be a useful approach in a broad area of applications, including data characterization, feature analysis, anomaly detection, image classification, and gamma-ray spectral analysis [17-20].

3.2 MCNP5-Geant4 Simulations

3.2.1 MCNP5 Simulation

The main interest in the present study is to take advantage of changes in the neutron energy spectrum due to differences in the level of uranium enrichment and to determine the UF_6 enrichment with an appropriate metric. It is also of interest to know if the characteristic features of the observed spectrum are dependent on UF_6 filling profile (the solidified UF_6 geometry); as mentioned in previous sections, other measurement techniques are sensitive to the filling profile. To this end MCNP5 was used to simulate the neutron transport through the UF_6 mass in a 30B cylinder. UF_6 filling profiles considered in [1] and shown in Figure 3.1 that may represent significant variability in the UF_6 mass distribution were used in the simulations. The simulated profiles range from a uniform shell geometry with 100% of the UF_6 mass distribution having a constant thickness along the 30B cylinder wall to a pooled geometry where 0% of the UF_6 mass

distribution has a constant thickness along the 30B cylinder wall. Intermediate profiles where 75%, 50%, and 25% of the UF_6 mass distribution with a constant thickness along the 30B cylinder wall were also considered. In all profiles considered, the total mass of the UF_6 was kept constant at the maximum shipping mass of a 30B cylinder, 2277 kg [12] and a 4.6 g/cm^3 UF_6 density was assumed.

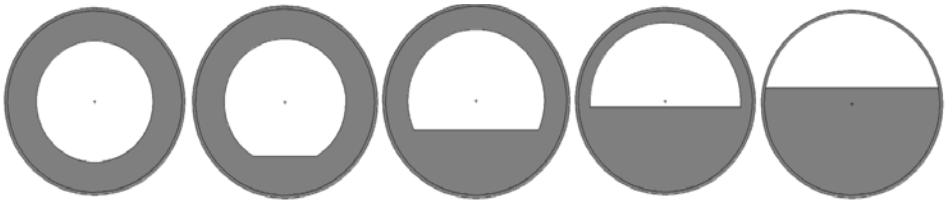

Figure 3.1. UF6 filling profiles used for 30B cylinder simulation [1]. Profiles considered range from shell geometry with 100% of the UF_6 mass having a constant thickness along the 30B container wall (left most profile) to pool geometry where 0% of the UF_6 mass has a constant thickness along the 30B wall (right-most profile). Intermediate profiles where 75%, 50%, and 25% of the UF_6 mass with constant thickness from the 30B wall were also considered. In all profiles considered the total mass of the UF_6 was kept constant.

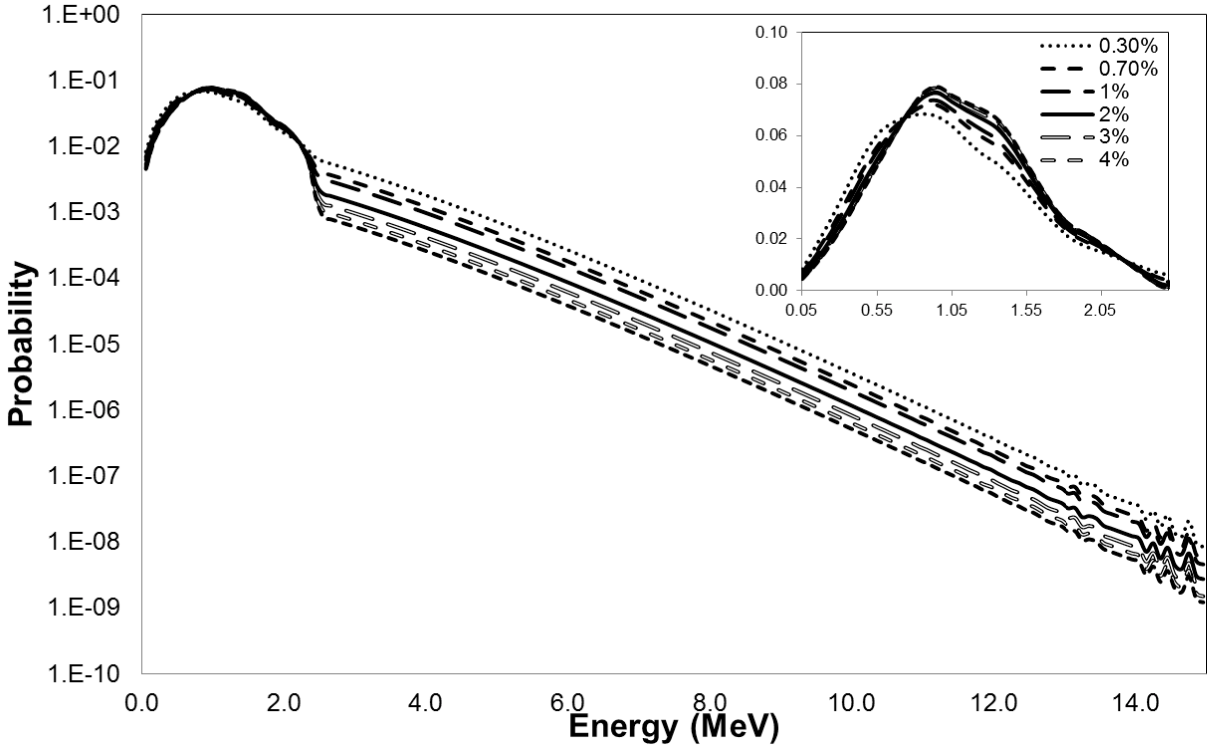

Figure 3.2. SOURCES 4C [11] calculated spontaneous fission (SF) and (α,n) neutron spectral distributions as a function of enrichment. The inset shows the variation in the (α,n) component for the different enrichments.

^{235}U enrichments of 0.3% (depleted uranium, DU), 0.718% (natural uranium), 1%, 2%, 3%, 4%, and 5% were considered in the simulations. The neutron source spectra for the different enrichments were based on the uranium isotopic fraction from [1]. Assuming linearity in the ^{234}U and the ^{235}U fractions, corresponding ^{234}U fractions for 1, 2, 3, and 4% ^{235}U enrichments were

determined. Table 3.1 shows the data for ^{234}U fraction as a function of ^{235}U enrichment. The isotopic fractions were then used in the SOURCES 4C [11] code to calculate the SF and the (α,n) neutron spectral distributions, shown in Figure 3.2, that were transported through the UF_6 mass and out of the 30B cylinder to a surface for subsequent Geant4 simulation. Figure 3.2 shows that as the enrichment increases, the fraction of events in the spectra above 2.5 MeV from SF decreases due to a strong increase in the $^{234}U(\alpha, n)^{19}F$ population. The (α,n) neutron distribution that is below 2.5 MeV and sitting on top of the ^{238}U SF continuous distribution also reveals a shift to higher energy for increased enrichment as shown in the inset. The shift is due to the increase in significance and energy of the α particles (4.859 MeV) from ^{234}U. At 0.3% enrichment, the α's from ^{238}U (4.27 MeV) are more significant and have a rate twice that of ^{234}U. At 5% enrichment, the α's from ^{234}U have a rate nearly eight times that of ^{238}U. In addition to the higher rate, the increment in the α energy (~0.589 MeV) will increase the neutron energy and therefore an observed shift in the spectrum. The total source neutron rate varied from 0.1085 neutrons/sec-cm^3 at 0.3% enrichment (DU) to 0.7219 neutrons/sec-cm^3 at 5% enrichment. The number of simulated source neutrons was constant for all enrichments and was calculated using the DU mass emission rate and a ten hour-equivalent measurement time. Higher enrichments were simulated for duration less than that of the DU due to their increased emission rate. For the 5% enrichment the neutrons simulated were equivalent to 1.5 hours measurement time.

Table 3.1. Isotopic fraction used in the SOURCES 4C code. A linear relationship was assumed to calculate the corresponding ^{234}U fraction for a given enrichment. Data was taken from Berndt et al. [1]

U-235	*U-234*	*U-238*
0.3	0.00232	99.69768
0.7	0.00544	99.29456
1	0.00778	98.99222
2	0.01558	97.98442
3	0.02338	96.97662
4	0.03118	95.96882
5	0.03898	94.96102

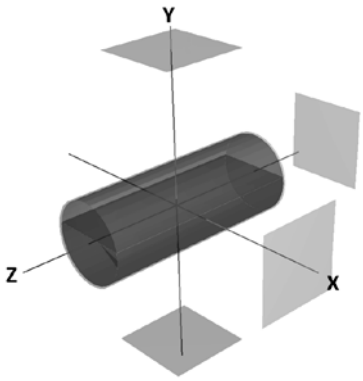

Figure 3.3. Source – detector setup geometry used in MCNP5 simulation. The four planes surrounding the 30B cylinder are located at the front face of liquid scintillator cell arrays considered in the simulations. MCNP5 PTRAC output was used to record position, momentum, and energy of outgoing neutrons at the four locations. These neutron histories were then resurrected in Geant4 simulations of the detector response.

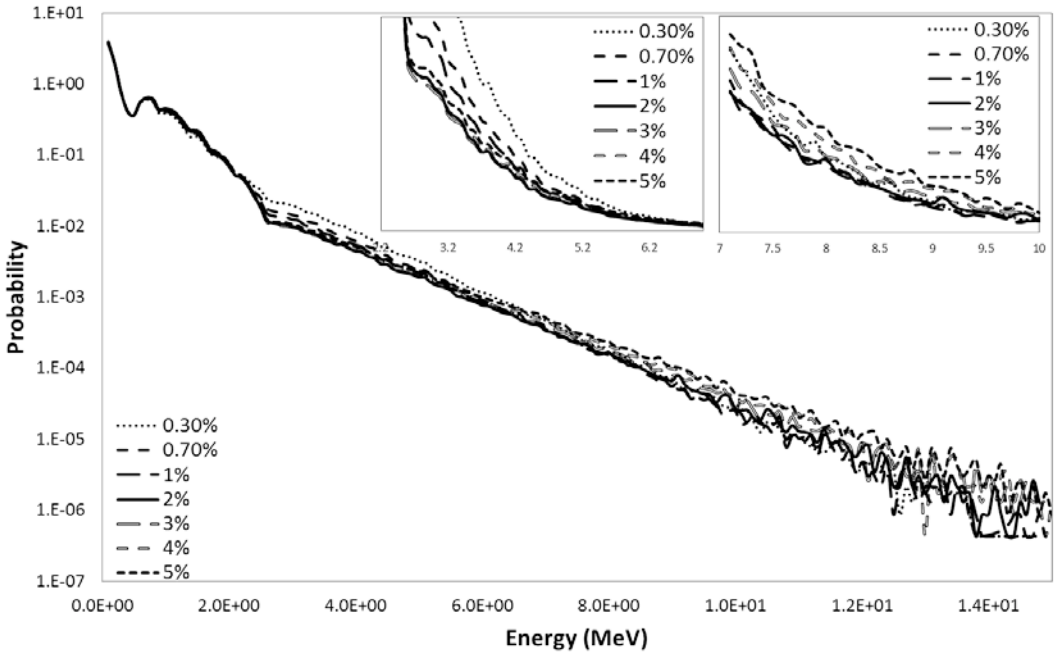

Figure 3.4. The energy spectra for neutrons exiting the 30B cylinder, along the Z-axis shown in Figure 3.3, and incident upon the liquid scintillators. As can be seen in the two insets, higher enrichments increasingly become significant due to induced fission neutrons at higher energies.

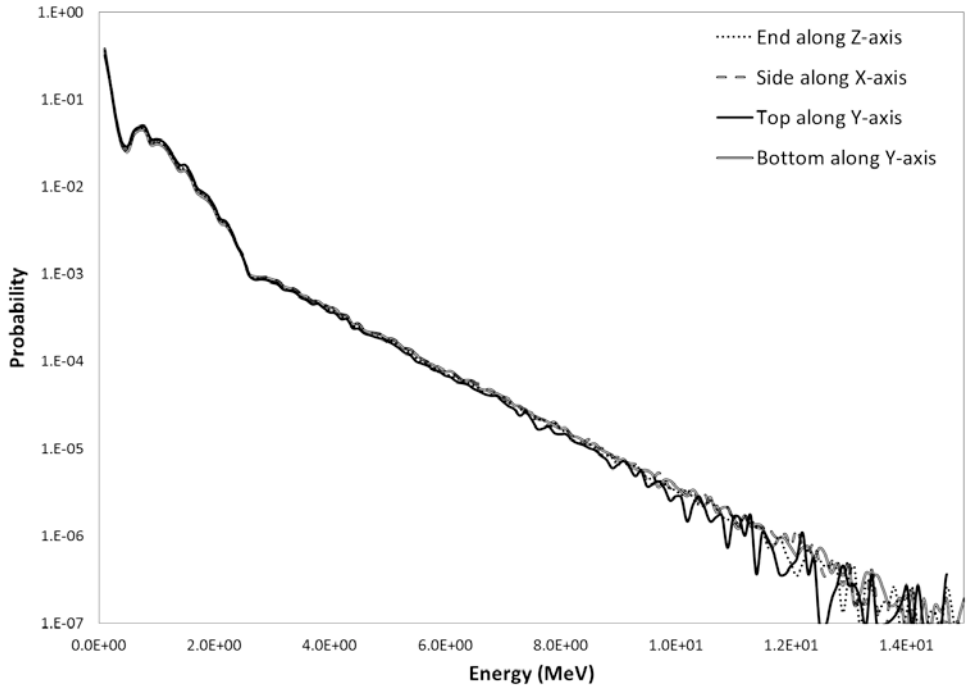

Figure 3.5. The energy spectra of neutrons exiting the 30B cylinder and incident at different tally planes (see Figure 3.3). The 3%-enriched energy spectrum for the pool profile reveals some location-dependent variations.

MCNP5 PTRAC output was used to record the position, momentum, and energy of neutrons at surfaces, shown in Figure 3.3, incident to the detectors in Geant4 simulation. The neutron spectral distributions emerging from a shell profile along the Z-axis are shown in Figure 3.4. The order in the plots, depicting different enrichments, changes at different energy regions as shown in the insets. Higher enrichments increasingly become significant at higher energies due to the induced fission neutrons. It was also observed that there exist slight differences in the spectral distributions for a given enrichment depending on the location of the setup. Figure 3.5 shows the spectral variation at the 3% enrichment for the pool profile.

3.2.2 Geant4 Simulation

Geant4.9.4 was used to transport neutrons inside the liquid scintillator detectors. Geant4 was chosen to allow particle discrimination of recoil protons from heavier charged particles, such as carbon, which is not possible using MCNP5. A total of sixteen right cylindrical liquid scintillator cells, each with 12.7 cm diameter and 5.08 cm length, were simulated at each location shown in Figure 3.3. The scintillator cells have the same geometric and material specifications of the front array of the Neutron Scatter Camera (NSC) developed by Sandia [14]. Using multiple cells in the detection provides good detection statistics in a relatively short measurement time by summing individual spectrum from each cell, while avoiding problematic pulse pileup from prevalent gamma rays in a given detection cell. However, it is crucial to confirm that differences in the observed spectra are exclusively statistical at a fixed location. The detector locations, shown in Figure 3.3, were chosen to study the variability of the source-to-detector geometry and therefore the impact on the PCA approach.

Neutron energy deposition in each scintillator cell was recorded and binned into 150 channels representing the neutron energy range 0 to 15 MeV. Based on the setup shown in Figure 3.3, for each enrichment with five different profiles and the sixteen liquid scintillator cells at each location, a total of 320 neutron spectra were simulated. Using the simulated spectra and the PCA technique, investigation was made to determine the spectral features' dependence on UF_6 enrichment and filling profile. Other factors that can possibly contribute to spectral features, mainly scattered neutrons from the surrounding environment and ambient gamma flux that can be misidentified as neutron pulses, were not considered. The impacts of these factors are topics for future investigations.

3.3 Application of Principal Component Analysis

PCA is a mathematical technique involving a procedure that transforms a number of correlated variables into uncorrelated variables called principal components (PC). The first principal component accounts for the maximum variability in the data and each succeeding components account for successively smaller fractions of the remaining variability [17-19]. The PCA technique has proven to be advantageous in various fields including data characterization, feature analysis, anomaly detection, image classification, and gamma-ray spectral analysis. The goals in the use of PCA are: reduction of dimension in the data, and identification of underlying meaningful variables or features in the data. The latter is the advantage we would like to exploit for UF_6 enrichment identification.

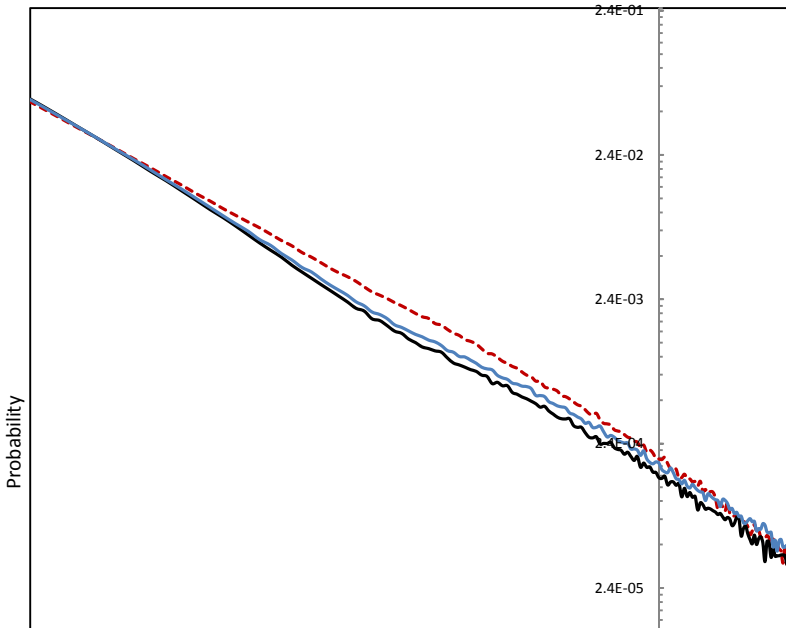

Figure 3.6. Neutron pulse height spectrum (PHS) for 0.3%, 3%, and 5% enriched UF_6. Measured light yield and energy resolution were used to calculate the PHS.

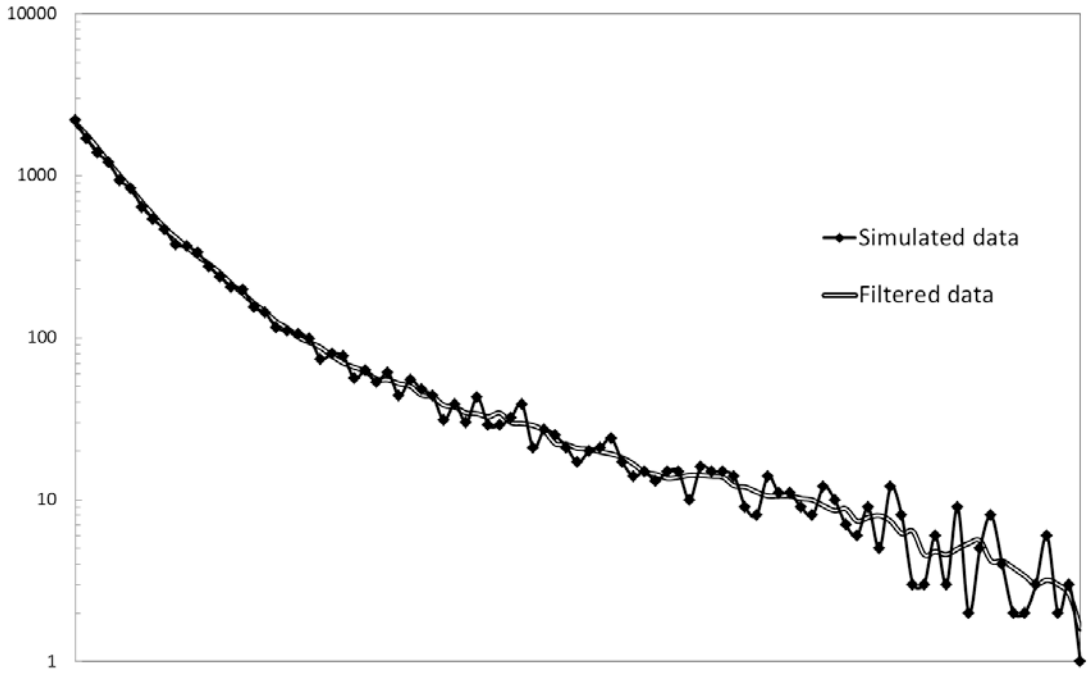

Figure 3.7. Neutron pulse height spectrum smoothed using Savitzky-Golay (SG) or polynomial filter [21]. The SG filter enables suppressing statistical fluctuation on neutron pulse height spectrum.

Before implementation of the PCA, the energy spectra from Geant4 simulation were processed using the measured light yield and energy resolution of the simulated liquid scintillators to

generate a realistic neutron pulse height spectum. Figure 3.6 shows representative simulated neutron pulse-height spectra for 0.3%, 3%, and 5% enriched UF_6 that were configured in a shell profile. It is obvious from the plot that the three enrichments represented are separated between 0.24 and 1.2 MeV. Above 1.2 MeV statistical fluctuation in the counts becomes increasingly significant. The increased variance above 1.2 MeV can have a significant impact in the PCA implementation. To address the impact, it may be necessary to use increased number of source neutrons in the simulation. This requires an increase in the measurement time of the UF_6 neutron spectrum. Alternatively, spectral smoothing can be used as an option provided the smoothing does not alter the underlying spectral features relevant to neutrons from the UF_6 mass. In the present study a low-pass filter known as Savitzky-Golay (SG) [21], or polynomial filter, was used to suppress the impact from statistical fluctuation. Figure 3.7 demonstrates the SG filter performance on a simulated spectrum. As can be seen on the figure, the variance at the higher energy end of the spectrum can be reduced using the SG smoothing. The lowest neutron energy considered in the analysis was 100 keVee. This was based on a typical threshold used in measurements [14]. The neutron pulse height spectrum was rebinned into ten energy groups that range from 0.1 to 7.5 MeV. Rebinning of the data was necessary due to the poor energy resolution of liquid scintillators, which make only a limited number of energy groups practical in feature extraction from the pulse height spectrum. The number of groups and group width can be flexibly varied to allow optimization in PCA implementation. A similar approach and detailed analysis was made using plastic scintillators in gamma-ray spectrometry by Ely *et al.* [22]. In the present study, a 100 keV bin width was used between 0.1 and 1 MeV. To allow statistically significant counts in all bins, a single bin was used for the energies between 1.0 and 7.5 MeV. Using the ten energy groups, applying the PC transformation will result in ten PCs.

The approach in the current PCA implementation assumes a reference PC transform, alternatively called a reference PC space, and is defined by a declared UF_6 enrichment in a 30B cylinder. For the present PCA implementation a 3% enrichment was used as the declared enrichment and therefore was used to train the PC transformation. Training of the PC transformation involves the evaluation of the coefficients and other related parameters used in the linear transformation. The coefficients—also known as the loading coefficients—are the eigenvectors calculated using the PCA implementation for the selected enrichment. Subsequent simulated or measured data from a 30B cylinder when transformed into the PC space may either be within the same PC distribution, if having 3% enrichment, or are identified as an outlier if the enrichments in the cylinders are different. This will allow anomaly detection in the simulated or measured spectrum. With the anomalous distribution, it may be possible to provide more information than simply the cylinder's material has an anomalous enrichment, and estimate the cylinder's enrichment using an appropriate calibration or metric. The Mahalanobis distance (MD) [23] is a common distance metric used in PCA implementation. The MD gives a variance-weighted distance for the projected PCs, or commonly known as PC scores, from the reference PCs and was used in the present study. After determining the PCs for each enrichment and profile, the MD was calculated between the reference PC scores and other enrichments of interest for each profile. The MD as a metric, or classifier, was used to generate the receiver-operating characteristic (ROC) curves for a given false positive probability (FPP) associated with misidentifying a given enrichment. Since a functional distribution cannot be associated with each enrichment's PC distribution, an order statistic, also known as a non-parametric statistic, was implemented in generating the ROC curves. The accuracy of the technique implemented can then be determined using the area under the (ROC) curve, AUC.

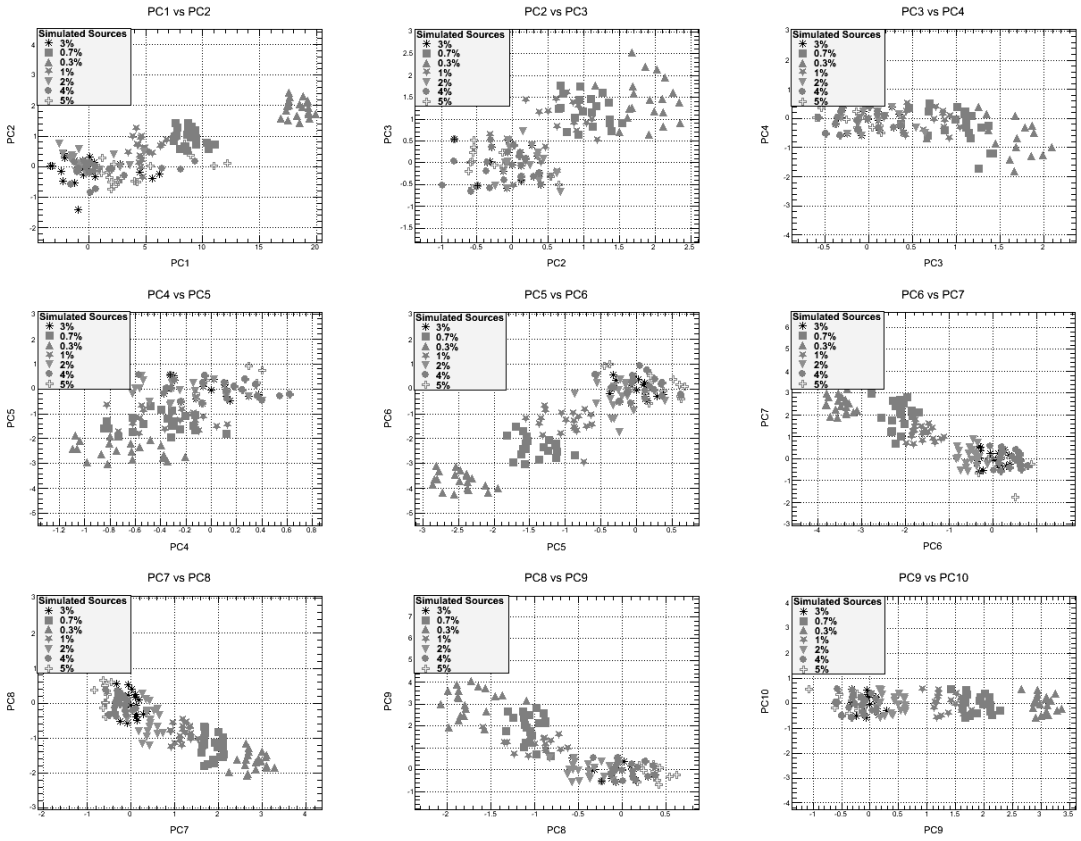

Figure 3.8. Plots of the ten PCs based on summing the response of all 16 detectors in each unique detection plane. The PC space was trained using all possible detector locations and UF_6 filling profiles, with a 3% declared UF_6 enrichment. Data was not smoothed in this analysis.

3.4 Results and Analysis

Initial PCA implementation proved that for each location considered in Figure 3.3, the differences in the neutron pulse-height spectra between the sixteen liquid scintillators cells are mainly statistical. Based on this finding, subsequent PCA implementation adopted a single detector approach in which all sixteen neutron spectra at a given location were summed to produce a single neutron pulse-height spectrum. Figures 16 and 17 present the plots of the ten PCs for the summed detector response arrangement before and after implementation of the SG filter, respectively. Individual enrichments are represented by twenty PC scores that are from the four locations and five profiles considered. The first PC has the most variance compared to the subsequent PCs. The variance in the PC scores can possibly be attributed to: differences in the geometry-related features from the four locations considered; characteristic features from the different neutron populations discussed in Section 3.1; variation in filling profiles; and statistical variance in the simulated neutron pulse-height spectra, mainly at higher neutron energies. Results from the present study show that statistical variance is a significant component in the calculated PCs. PC plots generated before the SG implementation, Figure 3.8, shows overlap between the reference 3% enrichment with adjacent enrichments for higher PCs. Relatively better separation

in the enrichments can be seen for lower PCs, as it the case for PC5 to PC8. The application of the SG filtering has enabled significant improvement in the separation of the 3% from the other enrichments. This is clearly evident in Figure 3.9, which shows the PC-space plots for the first five PCs. Almost all enrichments were discriminated from the 3% reference enrichment using the first two PCs. The improvement achieved using the SG filtering indicates that statistical noise in the neutron spectra has considerable impact in the PCA implementation. It can be seen that there is still some overlap between the 3%, the 4% and the 5% enrichments. This is most likely due to the statistical noise not addressed by the SG filter application. The overlap may result in reduced accuracy in classification of these enrichments using the MD metric.

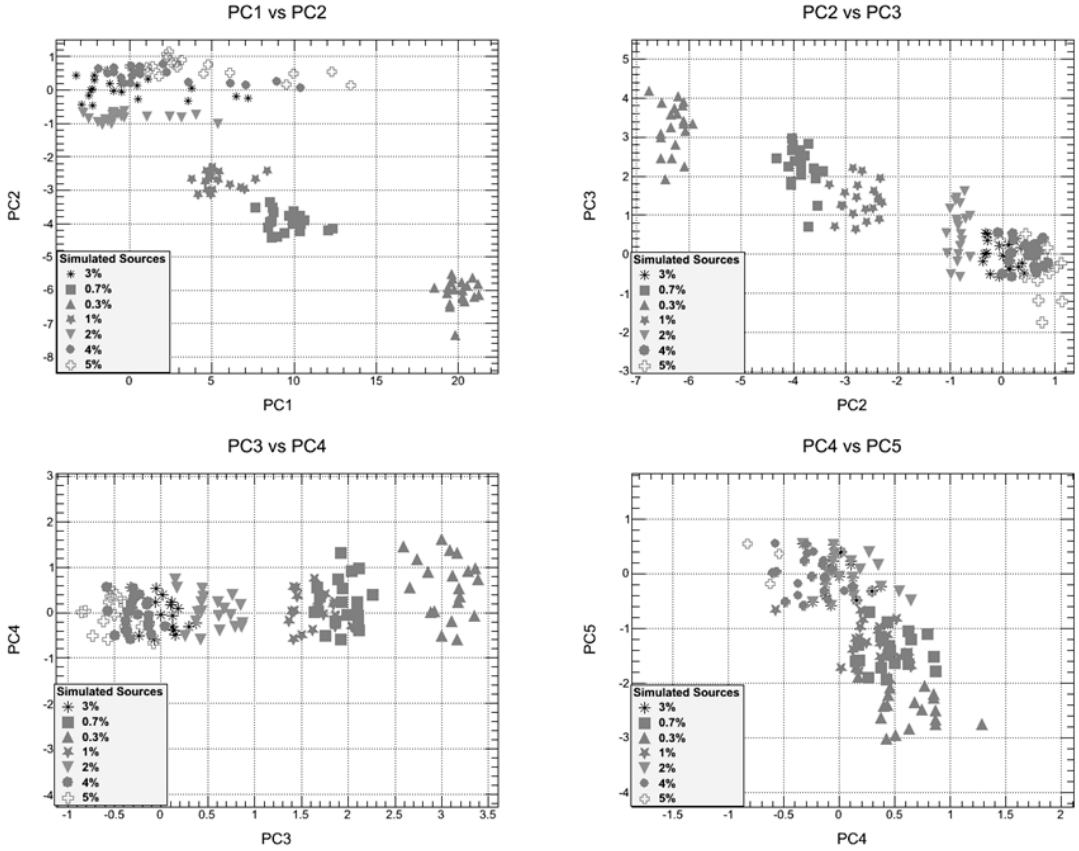

Figure 3.9. Plots using the first five PCs based on the summation of detector responses in each detection plane. The PC space was trained using all possible locations and profiles and with a declared 3% UF_6 enrichment. Data was smoothed using the Savitzky-Golay (SG) filter [21].

Figure 3.9 proves that the neutron pulse-height spectra may be represented by the first two PCs, which clearly show enrichment attributes associated with the neutron spectrum. At lower PCs (≥PC3), there is less information related to the enrichment attributes and the plots in Figure 3.9 reveal increasingly less discrimination among the different enrichments. Despite the significant variation in the UF_6 profile simulated, it was possible to discriminate the UF_6 enrichments. The approach in the present study has proved to be unaffected by the UF_6 filling profile. This further paves the way towards the fast monitoring and verification of UF_6 by enabling the design of efficient detection setup.

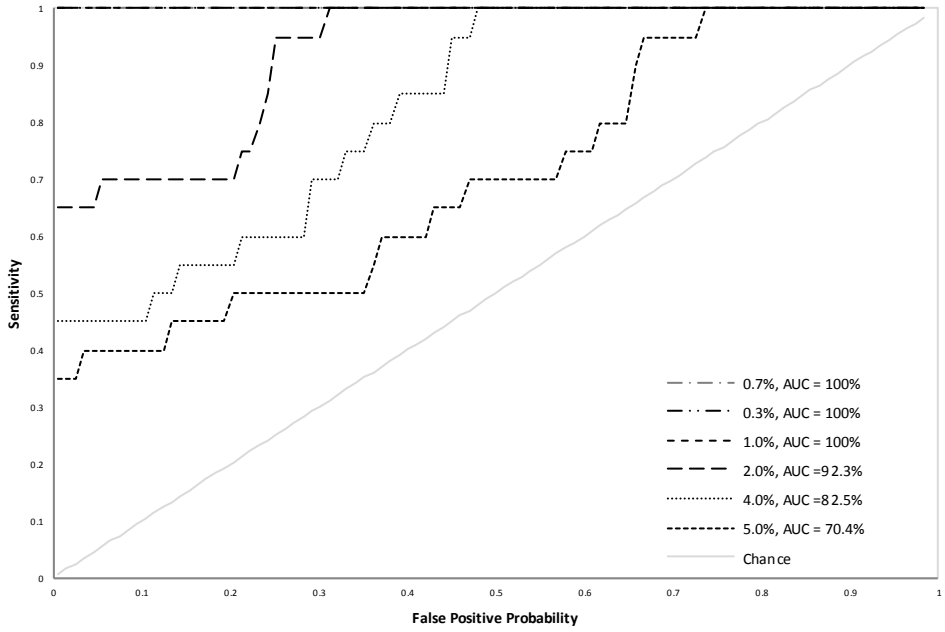

Figure 3.10. ROC curves generated using the first two PCs, which explain 79.4% of the total variance. Data was not smoothed in the analysis.

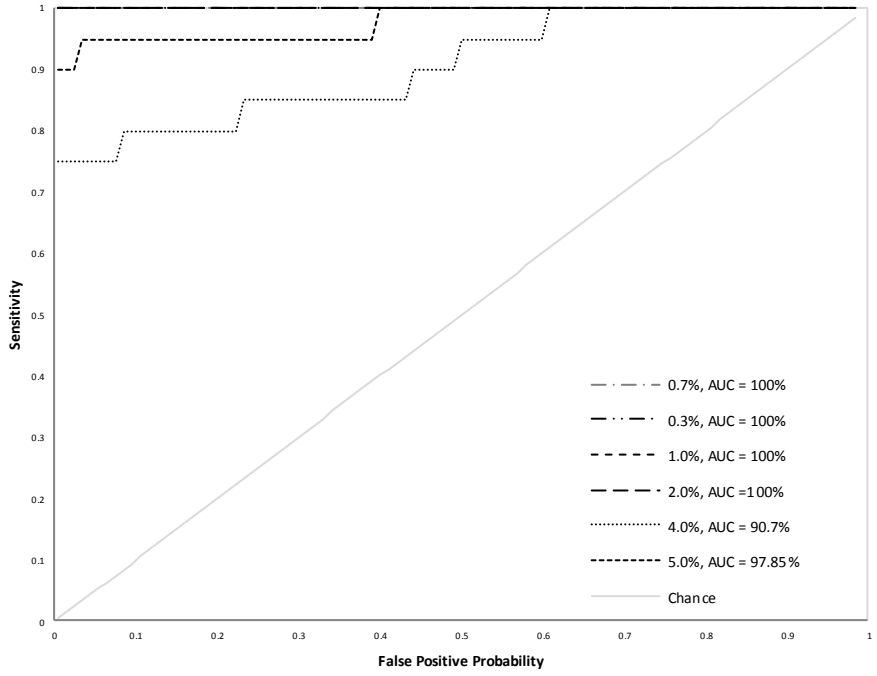

Figure 3.11. ROC curves generated using the first five PCs, which account for 94% of the total PC variance. Data was smoothed using the Savitzky-Golay [21] filter in this analysis.

Using the MD metric, ROC curves generated using the first five PCs for the data with no SG smoothing are shown in Figure 3.10. The Y-axis represents the sensitivity or the true positive and the X-axis represents the false positive also given as one minus specificity (true negative). The accuracy (AUC) in the classification of individual enrichments is shown in the legend. The first two PCs account 79.4% of the variance in the PC space. Including more PCs can possibly increase the accuracy. But this will be at the compromise of increasing dimensionality, and thus analysis complexity. Figure 3.11 shows the ROC curves generated using the first five PCs for the data with SG smoothing. The AUC is 100% for all except for the 4% and the 5%, which were determined to be 90.7% and 97.85%. The first two PCs account nearly 94% of the variance in the PC space.

3.5 Discussion

The present simulation study has demonstrated that neutron spectrometry coupled with an appropriate technique for feature extraction can allow unattended passive neutron assay, which is insignificantly affected by the UF_6 filling profiles or source-to-detector setup geometry. The outcome opens the possibility of fast monitoring and verification of UF_6 by enabling an efficient detector design. This in return allows reduced statistical variance in PCA implementation. PCA has been also demonstrated as one possible technique that can enable feature extraction and monitoring of UF_6 in storage cylinders. In the present study the simulated neutron spectra do not include features from scattered neutrons from specific measurement surroundings, misidentified gamma signals that can happen in PSD measurements, and background neutrons. These may have some impact in the PCA implementation. These and other factors will be topics for future investigations.

4. MEASUREMENT OF THE NEUTRON ENERGY SPECTRUM

4.1 Introduction

Monitoring uranium enrichment remains an important problem for nonproliferation and safeguards. Current technologies which measure the ^{235}U enrichment in UF_6 cylinders require controlled conditions for accurate measurements, and utilize gamma and low energy neutron signatures which measure only the outside surface of large, dense UF_6 volumes. This results in a non-robust measurement which could be exploited through diversion. As discussed in previous sections of this report, fast neutron spectrometry and imaging can be applied to fill this gap, as the high energy neutrons are deeply penetrating and carry the potential to allow for whole-cylinder measurements. While previous sections explored this measurement concept via simulation, here we will discuss a practical deployment of the technique. A suite of detectors was deployed at the Paducah Gaseous Diffusion Plant (PGDP) in July 2012, including several different liquid scintillator cells (EJ-309), a ^{3}He tube for simple neutron counting, and a large sodium iodide scintillator for gamma-ray spectroscopy. We will focus on the fast neutron response of the liquid scintillator and our efforts to characterize multiple UF_6 30B cylinders of varying enrichment using spectral information.

4.2 Experiment

Liquid scintillator was chosen because of its high detection efficiency, ability to discriminate between gammas and neutrons via pulse shape discrimination (PSD), and reasonable energy resolution. This has proven a successful combination in the past for the Neutron Scatter Camera [14], a detector which has been evaluated in this project for application to 30B cylinder assay. For the first measurement opportunity at PGDP, a measurement system that mimicked the important features of the Neutron Scatter Camera while affording maximum flexibility in deployment configuration and detector response information was desired. A system was constructed that contained EJ-309 cells of varying size to study the effect of cell size on the measurement. Included were 5.08 cm × 5.08 cm (diameter × height), 7.62 cm × 7.62 cm, 12.7 cm × 5.08 cm and 12.7 cm × 12.7 cm right cylindrical cells read out by either 5.08 cm or 12.7 cm Hamamatsu photomultiplier tubes (PMT).

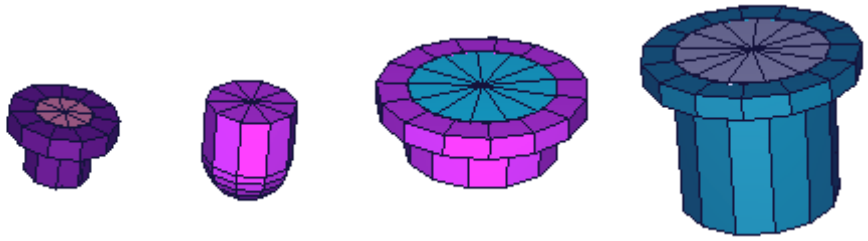

Figure 4.1. MCNP models of the 4 liquid scintillator cells, from smallest (5.08 cm × 5.08 cm) on left to largest (12.7 cm × 12.7 cm) on the right.

These detectors were arranged in a close-packed configuration and packed in Styrofoam and cardboard for robust shipping in a large crate. Signal and power were run out of the crate and to an electronics rack which utilized a Mesytec MPD-4 module to read out pulse amplitude and perform pulse-shape discrimination. A Mesytec-based analog data acquisition system was used

in lieu of a more compact system using waveform digitization because at the time of the measurement, this electronics choice closely resembled the configuration of the Neutron Scatter Camera.

The measurement area at PGDP is shown in Figure 4.2. This location is outdoors, far from a large background source of UF_6-filled 48Y cylinders. Generally, the measured cylinder was isolated from other 30B cylinders by moving cylinders into and from a fixed measurement location, with cylinders staged many 10s of meters away. A photograph of a typical measurement geometry is shown in Figure 4.3.

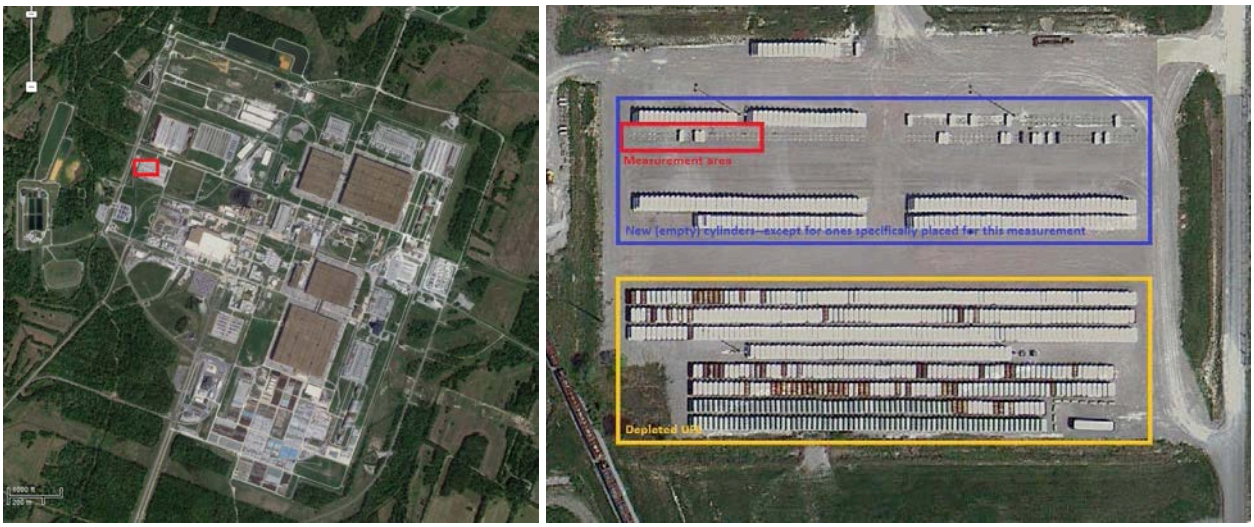

Figure 4.2. Left: an aerial view of PGDP taken from Google Maps, with the measurement area outlined in red. Right: a closer look at the measurement area; 30B cylinders intended for measurement were staged in the red area; other cylinders in the blue box were new, unfilled cylinders that would not contribute to background; the cylinders in the yellow box were filled with depleted UF_6.

Figure 4.3. A typical measurement configuration. The 30B cylinder is covered with lead blankets to reduce the gamma-ray contamination in the EJ-309 scintillator cells. The detectors are arranged in the blue box. The electronics rack is in the vertical crate seen on the left.

A total of seven 30B cylinders were measured with this detection system, ranging from 0.72% to 4.95% ^{235}U enrichment, including two cylinders containing down-blended Russian HEU. We positioned our detectors at distances up to 1 m from the cylinders, in side-on and end-on configurations. For the purpose of this comparison we will focus on 1 m distances in the side-on configuration, which was the most common measurement configuration. Lead blankets were also used in most cases to provide some photon shielding, although the shielding available made reproducibility difficult.

Calibrations were performed using isotopic sources in the field. A ^{60}Co source was used for energy calibrations, and a ^{252}Cf source was used for PSD calibrations. Each calibration was performed at least once per day.

Table 4.1. Paducah 30B cylinder enrichments.

Cylinder	*Enrichment*	*Origin*	*Measurement Time*	*Distance*
LU1511	0.72%	PGDP	6 hours	25 cm
LU1603	2.00%	PGDP	6 hours	1 m
LU2081	3.60%	PGDP	6 hours	1 m
LU2550	4.95%	PGDP	2.5 hours	1 m
LU0296	4.00%	Russian	1.5 hours	1 m
LU1004	4.95%	Russian	2 hours	1 m

4.3 Results

Data recorded for each cylinder consisted of energy and PSD in list mode for each detected event, allowing us to post-process the data and filter for neutron events before creating energy spectra. One common representation of this data is in an energy vs. PSD plot, which shows the neutron and gamma distributions. PSD is calculated as the area in the tail of the pulse to the area of the full measured pulse, and neutrons generally populate a horizontal band at a higher PSD value than do photons because the scintillation light generation for neutron events tends to have a slightly longer time scale. An example of this data for one of the cylinders is presented in Figure 4.4.

\ The high photon flux posed an issue for these measurements as pileup was common, and pileup will negatively influence PSD measurements. This effect is apparent when performing a PSD cut for neutrons and plotting the energy spectrum (Figure 4.5). Because of their larger volume for photon interactions, the larger cells suffered greatly in their ability to discriminate between gammas and neutrons, leaving the smallest 5.08 cm × 5.08 cm cell as the cleanest source of data. For this reason we focused further analysis on this cell.

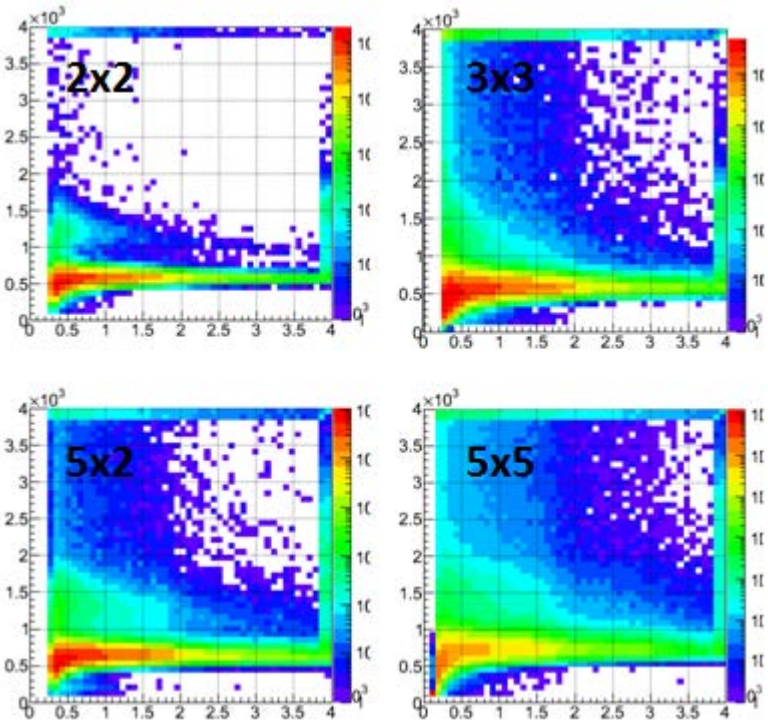

Figure 4.4. PSD (vertical axis) vs. energy (horizontal axis) for each liquid scintillator cell. Units are in amplitude (arbitrary units). Cell dimensions are listed in inches. The 2″×2″ cell (5.08 cm × 5.08 cm) can be seen to have the best PSD separation.

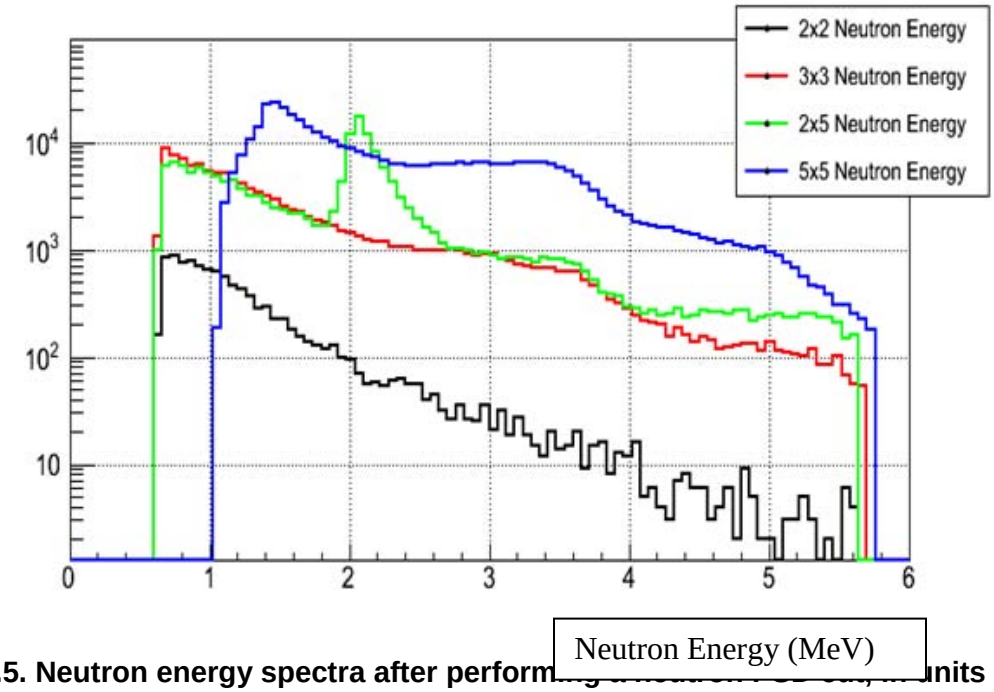

Figure 4.5. Neutron energy spectra after performing a neutron PSD cut, in units of MeV. A relatively smooth distribution is expected due to the poor energy resolution of liquid scintillator. Deviations from this can be attributed to gamma contamination.

Focusing on the 5.08 cm × 5.08 cm cell allows us to plot a relatively simple energy spectrum comparison of the different cylinder enrichments, shown in Figure 4.6. It should be noted that the cylinder with the smallest ^{235}U content cylinder (black line) has the highest fraction of events at large energies (as expected from the simulation studies); the highest enrichment (pink line) has the smallest fraction of events at large energies, which is because of the increasing $^{234}U(\alpha,n)^{19}F$ reaction and is also consistent with simulations.

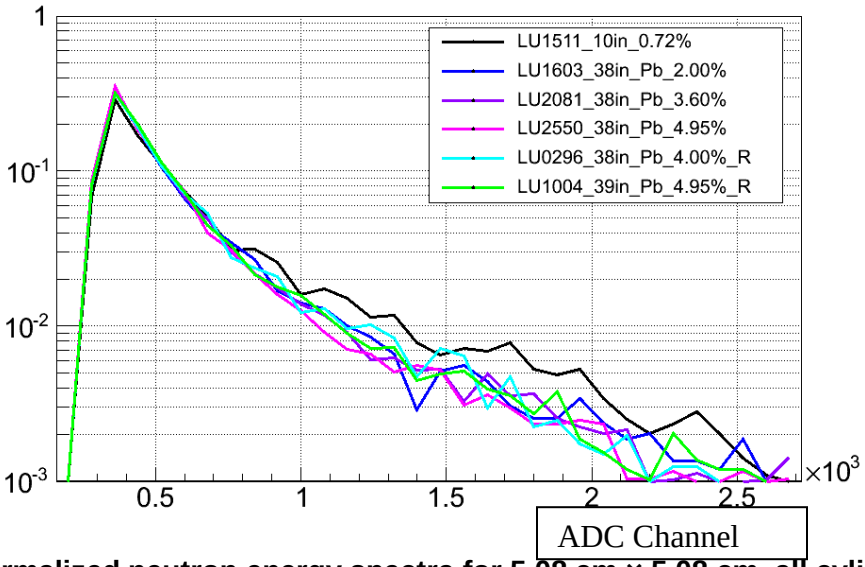

Figure 4.6. Normalized neutron energy spectra for 5.08 cm × 5.08 cm, all cylinders.

4.4 Analysis

Due to the fact that the ^{234}U enrichment increases the neutron population under 2.5 MeV, and the depletion of ^{238}U decreases the >2.5 MeV energy population, initial analysis focuses on a simple two energy window ratio method. All cylinders were expected to have the same mass, UF_6 filling profile, and similar systematic uncertainties from measurement geometry, so the PCA technique would not be required to filter out these sources of added measurement variance. To avoid a biased result, optimization of this window was initially done only with the four non-Russian material cylinders, using half of the available data up to a maximum of 3 hours. This optimized window fit was then applied to the other half of the data (up to 3 hours again), and the quality of the same data fitting function was tested. The optimization imposed the requirement of non-overlapping windows at least a few energy bins wide (see Figure 4.7), and looped through many of these possible combinations while the four non-Russian material data sets were fit to a linear function, with a test for goodness of fit. The ideal fit was selected to have both a large slope and a small χ^2 value. Figure 4.8 contains the optimized window results for the first half of the data set. The fit result was then applied to the second half-data set, shown in Figure 4.9.

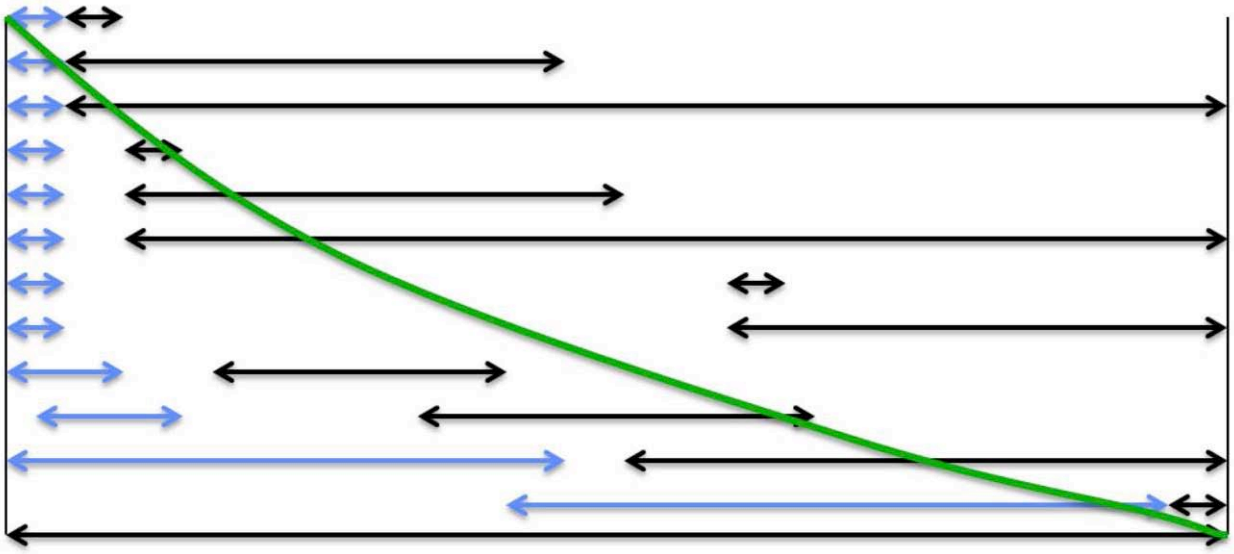

Figure 4.7. A schematic demonstrating the optimization of high-energy bins (black lines) and low-energy bins (blue lines) for a neutron energy spectrum (green curve). Each pair of blue/black lines depicts a possible binning combination that would be considered by the fitting routine. For each binning combination, a linear fit would be applied to the bin ratio vs. enrichment plot, and the best linear fit determines the optimal binning combination.

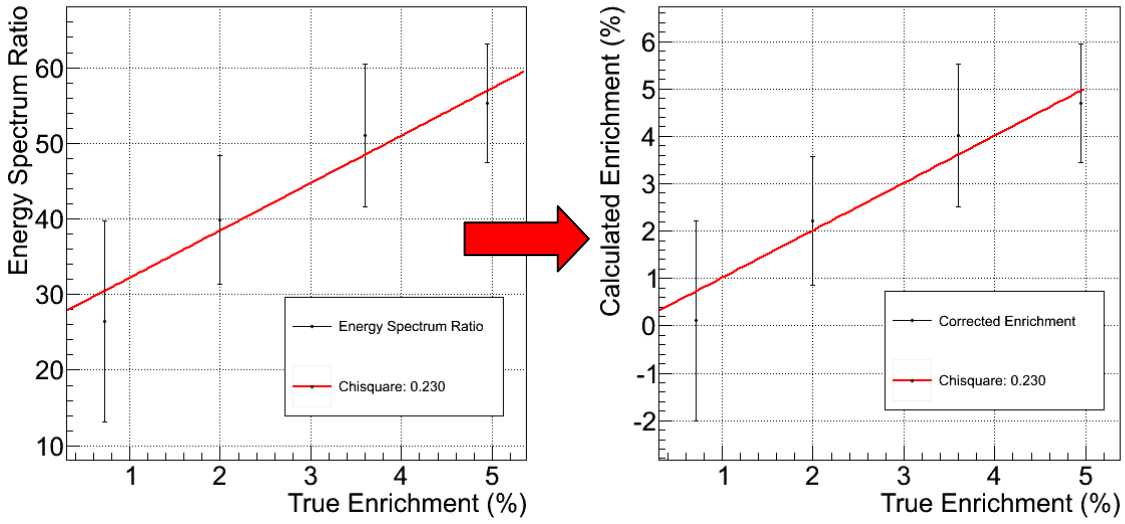

Figure 4.8. The first half of the data set with optimized windows. Left: bin ratio results vs. true enrichment. Right: plotting calculated vs. true enrichment using the inverse of the linear fit.

The prevailing error in the linear function fit was due to the high energy integral statistics, where 100 high energy neutrons were counted on average. The cylinders containing Russian down-blended HEU are not represented by the linear function generated by the other four cylinders. The typical uncertainty in these measurements is around 1.5% ^{235}U content.

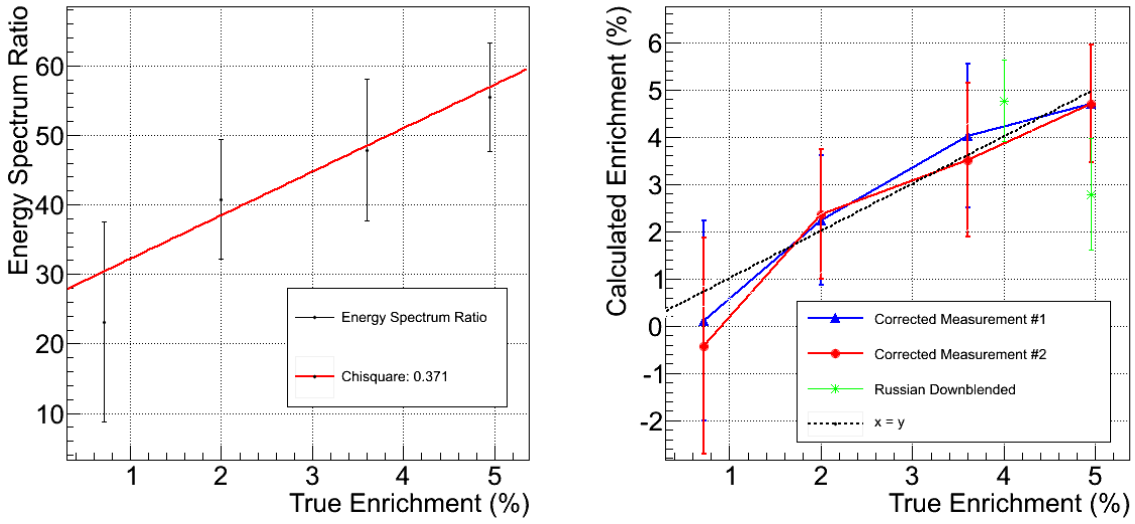

Figure 4.9. The second half-data set with energy windows optimized on the first half of the data. Left: the bin ratio results vs. true enrichment. Right: the calculated vs. true enrichment values for both halves of the run, with the Russian down-blended material cylinders shown as well.

4.5 Measurement system scaling

The measurement results from the PGDP deployment can be used to roughly size an array of EJ-309 liquid scintillator cells for future measurement of 30B cylinders. In Table 4.2, the data from the 5.08 cm × 5.08 cm cell is used to estimate the counting uncertainty as a function of measurement time if a single detector of the same size was placed 1 m from a 30B cylinder. A measurement period of 15 hours is required to reach a statistical uncertainty of 10% relative uncertainty. This is a very long measurement. However, Table 4.3 provides some hope. In this table, the detection volume is not fixed at a single small detector, and is instead scaled up to arrays of larger detectors. The relationship between number of detectors for a given cell size and counting time to achieve a 5% relative uncertainty is presented. For an array of twenty 12.7 cm × 12.7 cm detectors, the measurement will only take 10 minutes. This array would be very similar to a single plane of the Neutron Scatter Camera, so it is a practical goal.

4.6 Discussion

This series of measurements was performed in an attempt to show the viability of performing uranium enrichment measurements using neutron spectrometry. While only a small set of cylinders were used in this study, the results confirm that neutron spectroscopy can indeed be used to measure enrichment of UF_6.

Comparison of Figure 4.8 and Figure 4.9 indicates the neutron energy spectrum remained reasonably stable over a multiple-hour outdoor measurement, as the ratio test optimized on the data of Figure 4.8 also fits the data of Figure 4.9 within statistical uncertainty. The Russian down-blended material does not conform to this linear relationship, but it was not necessarily

expected to have the same neutron energy spectrum, as the isotopic content of ^{234}U is different in this material due to the initial enrichment to HEU with subsequent down-blending to LEU.

Further analysis of this data may reveal valuable information from the larger scintillator cells that can be extracted in time. Because the results obtained with this small detector array represent a statistically limited measurement often having fewer than 100 events in the high energy integral, future measurements are desirable with a larger array of detectors. Data presented in Table 4.2 and Table 4.3 indicate that reasonable measurement uncertainty could be achieved with a 10-minute counting time using an array of twenty 12.7 cm × 12.7 cm EJ-309 cells. Of course, the problem of photon pileup would need to be addressed, which may be achieved using waveform digitizers to identify and throw out pileup events in the analysis, engineered shielding on the detector, or a combination of both.

Table 4.2. The relationship between measurement time and measurement (counting) uncertainty for a single 5.08 cm × 5.08 cm cell placed 1 m from a 30B cylinder.

Time (hrs)	*High-energy counts*	*Uncertainty*
1	6.5	0.39
2	13	0.28
5	32.5	0.18
10	65	0.12
15	97.5	0.10
20	130	0.09
30	195	0.07
40	260	0.06
50	325	0.06
60	390	0.05

Table 4.3. The relationship between the number of cells in an array and measurement time to reach a 5% measurement (counting) uncertainty for cells of three sizes.

5.08 cm × 5.08 cm	*Hours*	*7.62 cm × 7.62 cm*	*Hours*	*12.7 cm × 12.7 cm*	*Hours*
1	50	1	14.8	1	3.2
2	25	2	7.4	2	1.6
5	10	5	3.0	5	0.64
10	5	10	1.5	10	0.32
15	3.3	15	1.0	15	0.21
20	2.5	20	0.74	20	0.16

5. PASSIVE NEUTRON IMAGING

5.1 Introduction

Current assay technology relies on the measurement of 186 keV gamma rays from ^{235}U decay or thermal neutron counting using ^{3}He detectors [1-2]. However, because of the short path length of these low-energy particles through the UF_6, both methods suffer from large systematic uncertainty due to incomplete knowledge of the mass distribution within the cylinder, in addition to being insensitive to material in the inner regions of the cylinder (see Figure 1.1).

It has been reported in [1] that the thermal neutron detector response is significantly dependent on the UF_6 the filling profile. Therefore knowing the filling profile in the UF_6 container may be important for the accurate assessment of UF_6 enrichment; even for penetrating fast neutrons, the number of neutrons counted over a fixed measurement interval has been calculated to vary when the distribution of material within the cylinder is changed (see Figure 5.1). This section of the report addresses the possibility of using passive fast neutron imaging to assess the material fill profiles in 30B cylinders. Models of the 30B cylinder with two distinct filling profiles were constructed and implemented for the purpose. In addition, we modeled the Sandia-developed Neutron Scatter Camera (NSC) to assess its ability to determine the UF_6 filling profile by fast neutron imaging. A detail of the imaging effort is presented below.

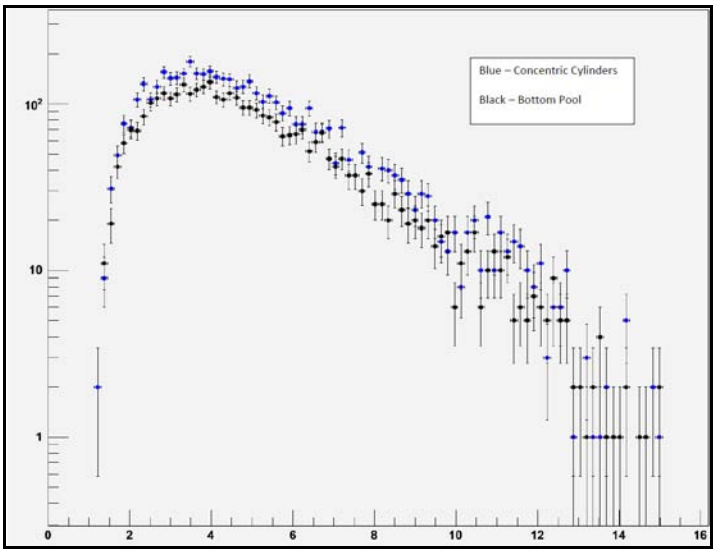

Figure 5.1. A simulation of the Neutron Scatter Camera response to a 30B cylinder filled in two geometries (shown in Figure 5.3 below) for UF_6 enriched to 5% ^{235}U. The simulation indicates the detector response is indeed affected by the geometry of a particular measurement scenario.

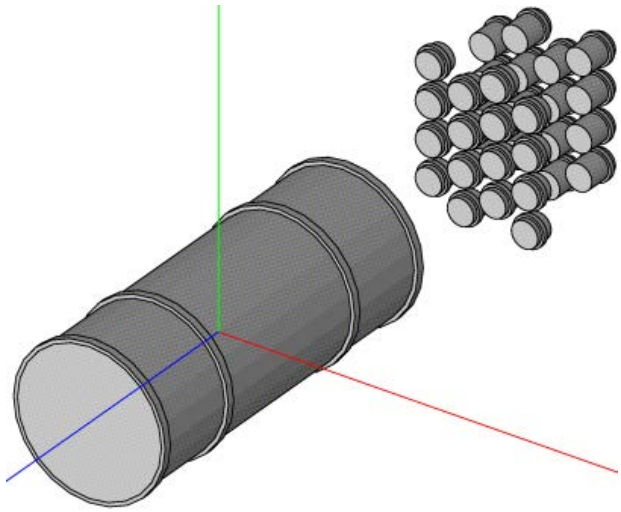

Figure 5.2. MCNP setup for imaging UF_6 30B cylinder using the Neutron Scatter Camera. The camera is set approximately two meters away from the center of the cylinder. The NSC consists of a front plane of 16 liquid scintillator detectors rear plane of 16 detectors placed up to 40 cm from the front plane; neutrons that scatter in both planes within an appropriate coincidence gate are used to reconstruct the neutron energy spectrum and image.

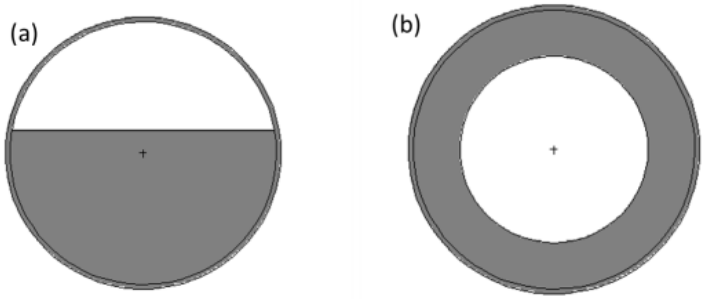

Figure 5.3. UF_6 30B cylinder material profiles used in modeling. (a) UF_6 (gray) solidified while the cylinder is lying horizontally, resulting in a fill from the bottom up with a void (white) at the top. (b) UF_6 solidified in a uniform shell on the cylinder wall, with a central void.

5.2 Methods

5.2.1 MCNP5 and MCNPX-PoliMi Modeling

MCNP5 [13] and MCNPX-PoliMi [24] were used to model the UF_6 30B cylinder and the NSC (shown in Figure 5.2). MCNPX-PoliMi was used to simulate the transport of fission and (α,n) neutrons through the UF_6 cylinder as well as their interaction with the NSC. Subsequently, appropriate detector response functions that account for the quenching and energy resolution of the NSC were implemented. Details of the NSC are given in previous publication [14,25]. Two distinct filling profiles for the 30B cylinder were considered (shown in Figure 5.3). These profiles have distinct geometries that can impact the UF_6 enrichment measurements.

5.3 Results and Discussion

5.3.1 Considering imaging for UF_6 profile determination

To assess the possibility of UF_6 profile determination through fast neutron imaging, spontaneous fission and (α,n) neutrons populations were generated using SOURCES 4C [11] and transported through the UF_6 mass using MCNP5 and MCNPX-PoliMi. The neutron energy flux that is incident on the NSC was recorded together with other relevant information including the position and momentum vectors for later analysis. Data from the MCNP5 PTRAC output file representing the incident neutron flux was back-projected to reconstruct the UF_6 profile image. The reconstructed image will help evaluate if the incident neutron flux has the required information to resolve the filling profile in the case of perfect detector response; subsequent simulations using real (imperfect) detector response will be degraded compared to this case, and so it can be considered an ultimate limit on performance. The back-projected images for the two distinctive profiles considered in the modeling are shown in Figure 5.4. As can be seen in the figure, fast neutron imaging has the potential to allow the assessment of UF_6 filling profile. However, it is clear from Figure 5.4(b) that pure consideration of back-projection image reconstruction is insufficient to determine whether the cylinder center is void or not. This may be a limitation of this analysis, as all of the neutrons detected from the cylinder, which has significant depth in the field of view compared to the detector standoff from the cylinder, are being projected onto a single plane. Assessment of the inner distribution may thus entail further image analysis.

Figure 5.5 is a Monte Carlo result mapping the origin of each fast neutron imaged by the NSC for the profile shown in Figure 5.3(b), confirming that fast neutron detection is sensitive to UF_6 throughout the entire cylinder. In this simulation, the NSC is located just to the left of the figure; the density of detected neutrons is greatest near the NSC, a combination of neutron attenuation while travelling through the UF_6 and solid angle coverage. A future study could attempt to correct for the non-uniform solid angle coverage of the NSC, thereby isolating the particle transport effects.

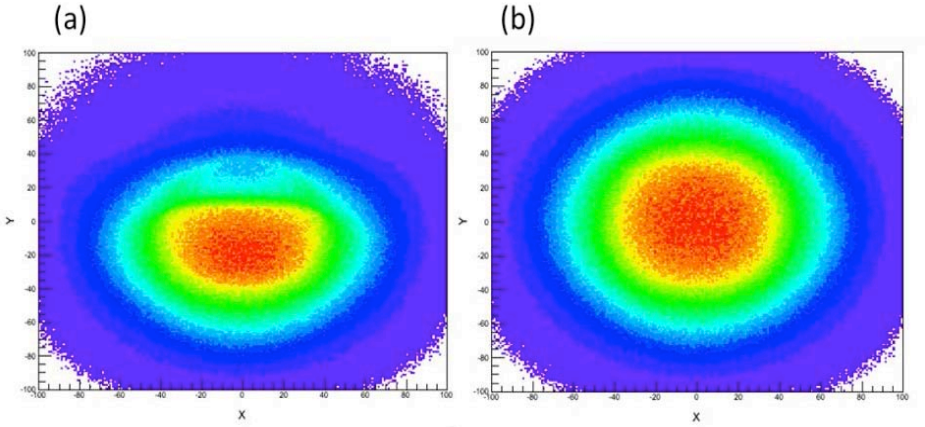

Figure 5.4. Back projected images for UF_6 30B cylinder filling profiles used in modeling. The geometries considered for (a) and (b) match the profiles shown in Figure 5.3, cases (a) and (b). The bottom-fill material profile (a) generates an image with suppressed intensity at the top, where the void is located. The symmetric material profile (b) generates an image that is uniform.

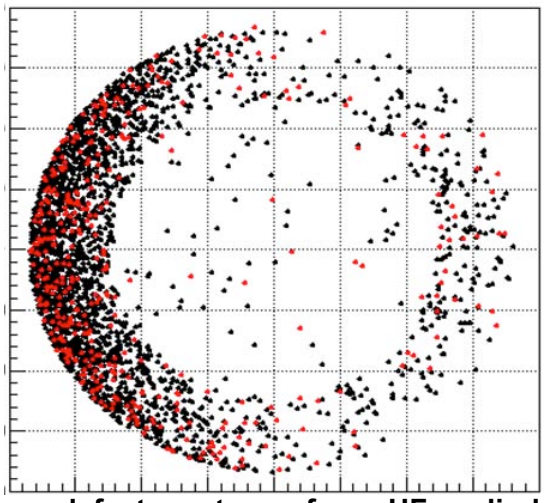

Figure 5.5. Origin of imaged fast neutrons from UF_6 cylinder shell with a constant thickness and with a void center. As can be seen, more neutrons are incident from the side facing the Neutron Scatter Camera (NSC), positioned 2 meters to the left of the cylinder. Fast neutrons from the opposite side of the shell, though not as abundant as ones on the NSC side, are also observed. Some neutrons appear to originate in the central void: these are actually from UF_6 material layered at the ends of the cylinder.

5.3.2 UF_6 profile imaging using the Neutron Scatter Camera

The NSC simulated data was used to reconstruct the UF_6 profile images. Details on the image reconstruction using the NSC may be found in [14,25]. UF_6 profile image reconstruction was performed using the filling profile shown in Figure 5.3(b) for the NSC positioned at the end of the 30B cylinder, as shown in Figure 5.2 and for the NSC positioned at the side of the 30B cylinder. Results from end and side views are shown in Figure 5.6(a) and (b) respectively. The results are encouraging when considering the end view. However, case (b) is not well resolved, and requires additional work.

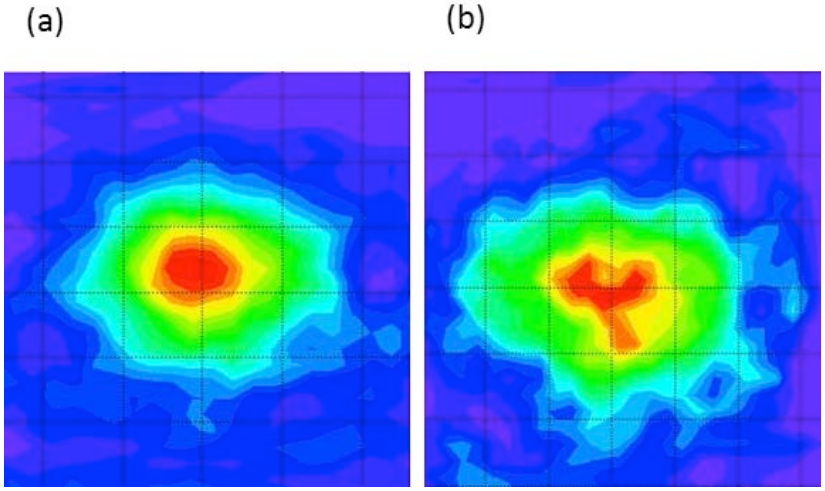

Figure 5.6. Neutron scatter camera (NSC) reconstructed images for (a) NSC facing the end of 30B cylinder as in Figure 5.2 (b) NSC facing the side of the 30B cylinder.

The possibility of using other imaging modalities may be considered in future work. While this paper focuses on the NSC because it is existing hardware at Sandia and is well-characterized, it is not necessarily the optimal instrument. For example, pinhole imaging systems have much finer position resolution than the NSC; these systems require consideration in the future of this project. Also, the double-scatter requirement imposed by the NSC for imaging events greatly reduces the population of available neutrons. Table 4.3 in the previous section indicated that an NSC-like array of detectors could perform spectroscopy with measurement times on the order of 10 minutes, but that is for all neutrons scattering in at least one detector, which is more efficient by up to two orders of magnitude. This implies that it might take 1000 minutes to image a cylinder with the NSC, which is an impractical measurement time at a facility with a high cylinder throughput.

5.4 Discussion

Passive fast neutron imaging for the determination of UF_6 fill profile in 30B cylinders has been considered for this project. Results obtained confirm that the information content of the neutron field is sufficient for a perfect imaging system to determine the UF_6 filling profile. This could be used in the future to reduce systematic uncertainties in the determination of UF_6 enrichment and mass in 30B cylinders, as well as other configurations and chemical compositions of dense special nuclear material. However, neutron detection optimization and imaging modalities have to be further investigated for unambiguous evaluation of UF_6 filling profile.

6. CONCLUSIONS

This project considered the use of fast neutron spectroscopy to perform uranium enrichment measurements on UF_6 storage containers, specifically the 30B product container. Simulations were performed to systematically step through the generation of neutrons in the bulk material, then transport neutrons through the 30B cylinder, and finally to simulate the detector response of the Neutron Scatter Camera (NSC). These simulations indicated that information on ^{235}U enrichment is contained in the neutron energy spectrum, and can be obtained with a good measurement. The simulations did not consider scattering off of the ground or other environmental effects; these effects may be considered for future work, although they are not expected to be important in calculating the NSC detector response, which is generally insensitive to scattered neutrons.

A measurement of several 30B cylinders was arranged at the Paducah Gaseous Diffusion Plant. An array of detectors representing NSC-like technology was assembled and used during these measurements. The data indicated that the neutron energy spectrum does indeed change with enrichment, and through the use of a simple two-bin analysis method, the change in the bin ratio as a function of enrichment could be observed. This measurement also was used to estimate the size of a reasonable prototype measurement system, which would be on the order of 20 individual 12.7 cm × 12.7 cm EJ-309 liquid scintillator cells (very similar to the NSC). A solution to photon pileup is required for such a system, though; this solution may use engineered shielding, or pulse digitization to sort out pileup events during the analysis. It may even be wise to consider a neutron spectrometer other than liquid scintillator—for example, spectrometers exist that utilize ^{4}He gas, and while they have excellent gamma-ray insensitivity, they are also much less efficient in neutron detection.

An advanced analysis technique (PCA) was investigated as a means to extract enrichment information when the systematic uncertainties—such as UF_6 filling profile—are unknown for a particular cylinder. The PCA technique was applied to a large set of simulated data, and it was found that PCA does allow identification of enrichment, regardless of detector location or UF_6 filling profile. A caveat is that the simulations assumed measurement times of several hours, which is likely to be impractical for field use. Studies of the tradeoff between PCA performance and measurement time are suggested for the future.

There are, of course, limitations to this measurement concept. The measurement precision is unlikely to ever challenge the performance of the enrichment meter [2], although the point of the neutron spectrometer is to reduce potential systematic uncertainties, which could potentially be large with the enrichment meter in uncontrolled measurement configurations. Also, the neutron spectrometry technique relies upon a well-characterized relationship between ^{234}U and ^{235}U isotopic fractions; however, the introduction of reprocessed uranium may complicate the analysis because the isotope ratios will be different after sufficient neutron irradiation in a reactor. The PGDP measurements indicate that this may have also been a problem when analyzing the cylinders containing Russian down-blended HEU, which does not have the same $^{235}U/^{234}U$ isotopic ratio as a result of its processing. It should be stated that these potential concerns and the photon pile-up experienced in the PGDP measurements are not unique to the proposed neutron spectrometry enrichment measurement: the gamma ray flux is a concern for all detectors except

those that are truly gamma-insensitive (such as ^{3}He proportional detectors), and the isotopic ratio will be a potential complication for any passive neutron-based measurement (including measurements based upon the conversion of neutrons into gamma-rays).

Finally, it is worth mentioning some other benefits of utilizing the NSC for the neutron spectrometry enrichment measurement. The NSC is capable of neutron imaging, as reported in Section 5, and it is possible to reject backgrounds—either a natural background or from nearby 30B cylinders—by performing neutron imaging during the measurement and rejecting neutrons that originate outside the region occupied by the cylinder being interrogated. Also, neutron imaging can potentially be used to image the UF_6 distribution within a 30B cylinder, which could provide a safeguards verification tool allowing inspectors to determine whether the cylinder has internal structure that is unexpected. The limited work on neutron imaging indicates that it might be possible, but would likely require further work to explore whether more efficient imaging techniques are possible due to the impractically-long imaging period required by the NSC.

7. REFERENCES

[1] R. Berndt, E. Franke, P. Mortreau, Nucl. Instr. and Meth. A (2010), doi: 10.1016/j.nima.2009.10.060

[2] ASTM Standard C1514, "Standard Test Method for Measurement of ^{235}U Fraction Using Enrichment Meter Principle," ASTM International, West Conshohocken, PA, 2008, DOI: 10.1520/C1514-08, www.astm.org.

[3] E. Franke, "Calculation of the neutron response for passive measurements," Report-No UF6-01/08, 2008.

[4] W.D. Ruther, T.F. Wang, and C.F. Hayden, "Uranium enrichment measurements without calibration using Gamma-rays above 100 keV," UCRL-JC-142832, 2001.

[5] K. A. Miller e*t al.*, "The Uranium Cylinder Assay System for Enrichment Plant Safeguards," LA-UR-10-02647, 2010.

[6] K. A. Miller, M.T. Swinhoe, H.O. Menlove, and J.B. Marlow, "Status Report on the Passive Neutron Enrichment Meter (PNEM) for UF_6 Cylinder Assay," LA-UR-12-21058, 2012.

[7] K. A. Miller, H.O. Menlove, M.T. Swinhoe, and J.B. Marlow, "Monte Carlo Feasibility Study of an Active Neutron Assay Technique for Full-Volume UF_6 Cylinder Assay using a Correlated Interrogation Source," *Nuclear Instruments and Methods in Physics Research Section A*, 703 (2013) pp. 152-157.

[8] E.K. Mace, L.E. Smith, Nucl. Instr. and Meth. A (2010), doi:10.1016/j.nima.2010.09.149

[9] R.B. Walton, "The Feasibility of Nondestructive Assay Measurements in Uranium Enrichment Plants," LA-7212-MS (1978).

[10] U.S. Department of Energy Office of Environmental Management, "Characteristics of Uranium Hexafluoride and its Compounds," http://web.ead.anl.gov/uranium/documents/factsheets/index.cfm, December 2001.

[11] W.B. Wilson *et al.*, "SOURCES 4C: A Code for Calculating (alpha,n), Spontaneous Fission, and Delayed Neutron Sources and Spectra," LA-UR-02-1839 (2002).

[12] R.I. Reynolds *et al.*, "American National Standard for Nuclear Materials—Uranium Hexafluoride—Packaging for Transport," ANSI N14.1-2001 (2001).

[13] F.B. Brown *et al.*, "MCNP VERSION 5," LA-UR-02-3935 (2002).

[14] N. Mascarenhas *et al.*, "A measurement of the flux, angular distribution and energy spectra of cosmic ray induced neutrons at fission energies," 2007 IEEE Nucl. Sci. Symp. Conf. Record, pp. 2050-2052.

[15] J. Brennan, E. Brubaker, R. Cooper, M. Gerling, C. Greenberg, P. Marleau, N. Mascarenhas, and S. Mrowka, "Measurement of the Fast Neutron Energy Spectrum of an ^{241}Am-Be Source Using a Neutron Scatter Camera," *IEEE Trans. Nucl. Sci.*, vol. 58, no. 5, pp. 2426-2430, Oct. 2011.

[16] J. Allison et al, "Geant4 developments and applications," *IEEE Trans. Nucl. Sci.*, vol. 53, no. 1, pp. 270-278, 2006.

[17] K. Fukunga, "Statistical Pattern Recognition," *Morgan Kaufmann*, 2nd edition, 1990.

[18] I.I. Jolliffe, "Principal Component Analysis," *Springer Verlag Series*, 2nd Edition, 2002.

[19] K. Webb, "Statistical Pattern Recognition," *John Wiley & Sons*, 2nd edition, 2002.

[20] R.C. Runkle, M.F. Tardiff, K.K. Anderson, D.K. Carlson, "Analysis od spectroscopic radiation portal monitor data using principal component analysis," *IEEE Trans. Nucl. Sci.*, vol. 53, no. 3, pp. 1418-1423, June 2006.

[21] A. Savitzky and M.J.E. Golay, "Smoothing and differentiation of data by simplified least square procedure," *Anal. Chem.*, vol. 36, pp. 1627-1639, 1964.

[22] J.H. Ely, R.T. Kouzes, B.D. Geelhood, J.E. Schweppe, and R.A. Warner, "Discrimination of naturally occurring radioactive material in plastic scintillators," *IEEE Trans. Nucl. Sci.*, vol. 51, no. 4, pp. 1672-1676, August 2004.

[23] P.C. Mahalanobis, "On the generalized distance in statistics," *Proceedings National Institute of Science*, India , vol. 2, no. 1, pp. 49-54, January 1936.

[24] S. A. Pozzi, E. Padovani, and M. Marseguerra, "MCNP-PoliMi: A Monte Carlo Code for Correlation Measurements," *Nuclear Instruments and Methods in Physics Research Section A*, 513/3 pp. 550-558, 2003.

[25] J. Brennan, K. Krenz, N. Mascarenhas, P. Marleau, and S. Mrowka, "Results with the neutron scatter camera," *IEEE Trans. Nucl. Sci.*, vol. 56, no. 3, pp. 1269-1273, Jun. 2009.

DISTRIBUTION

1	MS0359	D. Chavez, LDRD Office	Org. 07911
1	MS0899	Technical Library	Org. 09536 (electronic copy)
1	MS1371	Dianna Blair	Org. 06832
1	MS9004	Jim Lund	Org. 08130
1	MS9406	Erik Brubaker	Org. 08132
1	MS9406	Mark Gerling	Org. 08132
1	MS9406	Scott Kiff	Org. 08132
1	MS9406	Peter Marleau	Org. 08132
1	MS9406	Wondwosen Mengesha	Org. 08136
1	MS9406	Stanley Mrowka	Org. 08131
1	MS9406	Craig Tewell	Org. 08132
1	MS9408	Isaac Shokair	Org. 08123


Sandia National Laboratories